Rare Met. (2024) 43(6):2498–2526
https://doi.org/10.1007/s12598-023-02591-8

RARE METALS

REVIEW

Application of UiO-66 and its composites for remediation and resource recovery of typical environmental contaminants: a review

Hui-Min Zhang, Yun-Long Wang, Xin-Feng Zhu*, Zhen-Zhen Huang, Dan-Dan Pang, Kai Wang, Chao-Hai Wang*, Zhong-Xian Song, Shi-Qiang Yin, Lin-Lin Chang, Jin-Hui Zhang*

Received: 21 May 2023 / Revised: 26 July 2023 / Accepted: 30 July 2023 / Published online: 26 February 2024

Abstract UiO-66 series metal–organic framework materials (MOFs) are typical porous materials assembled by Zr^{4+} with a large mass-to-nucleus ratio and terephthalic acid ligands, which form tetrahedral and octahedral cages arranged in a periodic triangular window pattern. Due to the strong interaction between Zr and O, UiO-66 series MOFs exhibit high thermal stability, structural stability, and chemical stability. This article mainly reviews the applications of UiO-66 and its composites in adsorption, photocatalysis, and resource utilization, while exploring the harm of pollutants to human health and the environment. In the first part, the differences in adsorption and removal mechanisms of liquid organic pollutants, heavy metals, and volatile organic compounds (VOCs) are investigated. The results show that organic pollutants are mainly removed by physical adsorption, electrostatic interactions, hydrogen bonding, and π-π interactions, while heavy metals are mainly removed by chemical adsorption, electrostatic interactions, reduction, and chelation. VOCs are mainly removed by the pore volume and pore size structure of the material. Heterojunction catalysis can achieve non-toxic treatment of pollutants, and this study mainly focuses on UiO-based composite materials constructed by strategies such as semiconductor composites, ion doping, and metal/dye encapsulation. In the second part, the synergistic effect between the components of UiO-based composite materials promotes the oriented and rapid separation and transfer of carriers at the material interface, thereby promoting the generation of active species such as h^+, $\cdot O_2^-$ and ·OH, and achieving rapid degradation of pollutants and detoxification of heavy metals. In the third part, heterojunctions can realize the resource utilization of pollutants in water and air, producing energy-type substances such as hydrogen and methanol while solving environmental problems. In addition, this article also summarizes the harm of common typical pollutants to the environment and human health. Finally, the development prospects and unresolved problems of UiO-66-based materials in water remediation, gas purification, and environmental resource utilization are reviewed.

Keywords UiO; Adsorption; Photocatalysis; Environmental pollution; Resource recovery

H.-M. Zhang
School Infirmary, Henan University of Urban Construction, Pingdingshan 467036, China

Y.-L. Wang, X.-F. Zhu*, Z.-Z. Huang, D.-D. Pang, K. Wang, C.-H. Wang*, Z.-X. Song, S.-Q. Yin, L.-L. Chang, J.-H. Zhang*
Faculty of Environmental and Municipal Engineering, Henan Key Laboratory of Water Pollution Control and Rehabilitation Technology, Key Laboratory of Carbon Emission Reduction and Combined Air Pollution Control Technology, Henan University of Urban Construction, Pingdingshan 467036, China
e-mail: zhuxf780@163.com

C.-H. Wang
e-mail: chaohai@hncj.edu.cn

J.-H. Zhang
e-mail: jhzhang018@163.com

K. Wang
School of Resources & Environment, Collaborative Innovation Center of Coalbed Methane and Shale Gas for Central Plains Economic Region, Henan Polytechnic University, Jiaozuo 454003, China

J.-H. Zhang
The Key Lab of Pollution Control and Ecosystem Restoration in Industry Clusters, Ministry of Education, Guangzhou Higher Education Mega Centre, South China University of Technology, Guangzhou 510006, China

1 Introduction

With the rapid development of society, global climate change, environmental pollution (organic pollutants in water bodies, volatile organic pollutants in the atmosphere), and energy shortages have attracted people's attention [1]. Wastewater pollution mainly caused by organic dyes, antibiotics, and heavy metals, as well as atmospheric pollution mainly caused by carbon dioxide (CO_2) and volatile organic compounds (VOCs), not only seriously endanger human health but also severely damage the ecological environment. Therefore, their treatment is urgent. Currently, commonly used technologies for the purification of typical pollutants in the environment include adsorption, catalysis, and bioremediation [2–5]. In the first year of China's "the 14th Five-Year Plan", "Carbon Peak and Carbon Neutrality" was proposed. Photocatalytic CO_2 utilization is considered as a potential decarbonization technology. Facing the dual problem of water scarcity and water pollution, photocatalytic technology can not only achieve detoxification/degradation of environmental pollutants but also produce energy materials such as hydrogen, which has attracted a lot of attention from researchers [6, 7]. As the indoor air environment on which humans rely for a lot of time to survive, the presence of VOCs seriously affects human health. Adsorption and photocatalysis can remove pollutants and purify the indoor environment under mild conditions [8–10]. Therefore, based on the actual situation, the development of adsorption and photocatalysis technologies with mild reaction conditions is timely, and the development of efficient adsorption or photocatalytic materials is crucial.

Currently, researchers are committed to developing new materials with high adsorption capacity and catalytic activity to remove pollutants from water and air, while achieving resource utilization of pollutants. Metal–organic framework materials (MOFs) assembled from metal nodes and organic ligands are widely used in gas adsorption, storage, sensing, catalysis, and drug release due to their large specific surface area, tunable pore structure, and controllable morphology [11–15]. In addition, the semiconductor properties of MOFs make them attractive in the fields of photocatalytic hydrogen production, CO_2 reduction, organic degradation, and heavy metal reduction [16–19]. Importantly, compared with traditional porous materials such as activated carbon, molecular sieves, and mesoporous silica, MOF materials not only have higher specific surface area, ease of structural functionalization, and porous structure conducive to pollutant mass transfer and adsorption, but their semiconductor properties are also beneficial for photocatalytic pollutant removal [20]. UiO-66 ($[Zr_6O_4(OH)_4(bdc)_{12}]$) is a popular UiO series MOF material that has been widely studied due to its high specific surface area, excellent structural stability, connected three-dimensional (3D) structure, and photo-responsiveness [21]. UiO-66 is a representative microporous MOF material composed of a Zr^6 octahedron linked to 12 terephthalic acid ligands, forming tetrahedral cages and octahedral cages [22]. In the Zr^6 cluster of the octahedron, six vertices are occupied by Zr^{4+}, and eight triangular faces are covered by four μ_3-OH and four μ_3-O. The $[Zr_6(\mu_3\text{-}O)_4(\mu_3\text{-}OH)_4]$ nucleus is further capped by twelve carboxylic acid groups to form the $[Zr_6(\mu_3\text{-}O)_4(\mu_3\text{-}OH)_4(COO)_{12}]$ cluster. The UiO-66 series materials are composed of tetrahedral cages ($\sim$ 1.1 nm) and octahedral cages ($\sim$ 0.8 nm) arranged periodically through triangular windows ($\sim$ 0.6 nm), with a ratio of 1:2 [23]. In addition, compared with the more stable zeolitic imidazolate framework (ZIF) and Materials of Institute Lavoisier (MIL) series MOF materials reported in the literature, the secondary structural units formed by the Zr^6 cluster have inertness and structural stability under various chemical conditions due to the inherent oxygen affinity of Zr^{IV} [24, 25]. Meanwhile, UiO-66 materials with various functional groups, such as UiO-66-NO_2, UiO-66-Br, UiO-66-Cl, UiO-66-COOH and UiO-66-NH_2 (Fig. 1), have also been synthesized and applied in the fields of environmental purification and resource utilization through post-synthesis or one-step synthesis [26, 27]. To achieve in-situ adsorption-catalytic degradation of pollutants, researchers have combined various types and morphological structures of semiconductors with UiO-66 materials, and the resulting materials have been widely used in hydrogen production, CO_2 reduction, organic degradation, heavy metal reduction, and other fields [28–31].

Over the past decade, various researchers have utilized UiO-66 series materials in different research fields such as adsorption, catalysis, and drug release. At the same time, several papers on UiO-66 series MOFs have also been published, exploring their application in the fields of environmental purification or resource utilization. Ahmadijokani et al. [32] used UiO-66 materials for the adsorption/separation or degradation/reduction of organic pollutants in liquid phase, while Usman et al. [33] systematically investigated the research progress of UiO-66 series materials in CO_2 capture, separation, and resource utilization. Winarta et al. [34] mainly reported on the synthesis, structural defects, and functional stability of UiO-66, while Zou et al. [35] explored the application of UiO-66 series materials from the aspects of material synthesis and functionalization, especially UiO-66. Numerous review articles and research papers indicate the rapid development and great potential application value of UiO-66 series materials. However, the adsorption and catalytic mechanisms of gas-phase pollutants and liquid-phase pollutants are not completely consistent, and there is an urgent

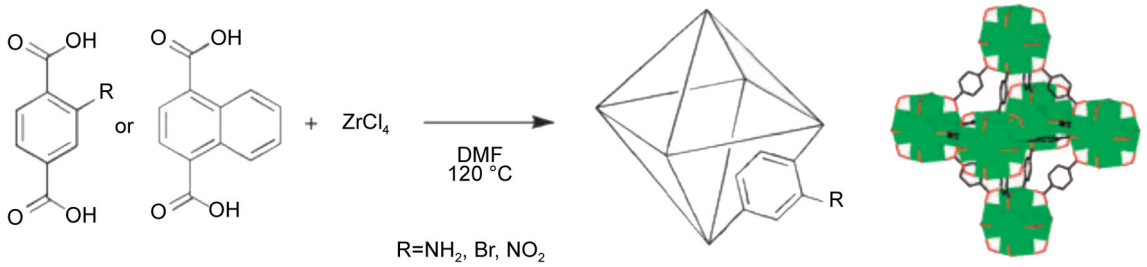

Fig. 1 Synthesis of isoreticular UiO-66 functionalized analogues UiO-66-NH_2, UiO-66-Br, UiO-66-NO_2 (R=NH_2, Br, or NO_2), and UiO-66-1,4-Naph, where UiO-66 framework with its Zr_6O_6 cuboctahedron SBU (green) is schematically represented as an octahedron. Reproduced with permission from Ref. [24]. Copyright 2010, Royal Society of Chemistry

need for timely and systematic review of recent relevant research progress to break through the limitations of current material applications. Therefore, this paper systematically explores the research progress of UiO-66 based materials in the fields of environmental and resource utilization, including pore structure, specific surface area, structural stability, hydrophobicity, and semiconductor properties, providing theoretical guidance for the design of structurally stable materials and basic data for the effective removal of pollutants.

2 UiO-66 for adsorption of environmental pollutants

Adsorption technology is widely used for the removal of pollutants in the environment due to its advantages such as simple processing, high efficiency, and economic feasibility [36]. Commonly used adsorbent materials include activated carbon, biochar, zeolite and clay [37]. MOFs materials are more favorable for the adsorption and enrichment of pollutants than these traditional porous materials because of their richer and adjustable pore structures and extremely large specific surface area [38]. Therefore, the development of MOFs materials with high adsorption capacity, adsorption rate, and desorption rate plays a crucial role in the removal of pollutants.

2.1 UiO-66 for adsorption of organic pollutants in liquid phase

The extensive use of dyes or pigments in processes such as textiles, printing and dyeing, and leather has resulted in pollutants being discharged into water bodies exceeding the environment's self-purification capacity, leading to a significant deterioration in water quality. Adsorption is considered an economical and efficient treatment technology for water pollution, mainly relying on the electrostatic interaction, π-π interaction, hydrogen bonding, or physical adsorption of materials to remove pollutants [39–41]. However, organic pollutants in water bodies do not exist in a single form but coexist in multiple forms, and there are situations where charges are opposite, making it extremely challenging to simultaneously remove dyes with opposite charges. Ahmadijokani et al. [39] used UiO-66 materials with good structural stability for the selective adsorption and removal of four dyes, including Methyl Red (MR), Methyl Orange (MO), Methylene Blue (MB), and Malachite Green (MG). The results showed that under low pH conditions, UiO-66 had a higher adsorption capacity for anionic dyes than cationic dyes. The maximum adsorption capacities of MR, MO, MB and MG were 384, 454, 133 and 370 $mg \cdot g^{-1}$, respectively. Meanwhile, in mixed dyes, UiO-66 could selectively adsorb anions (Fig. 2). The adsorption mechanism results showed that the interactions between UiO-66 and anionic and cationic dyes were electrostatic interaction, hydrogen bonding, π-π interaction, physical adsorption, and pore adsorption of UiO-66. Embaby et al. [40] explored the selective adsorption performance of UiO-66 for anionic and cationic species by investigating the differences in adsorption of anionic dyes and cationic dyes by UiO-66. The result was consistent with most literature reports. UiO-66 selectively adsorbed anionic dyes, which was mainly due to the positive Zeta potential of UiO-66 surface, facilitating the adsorption of anionic dyes. Therefore, the adsorption capacity of Alizarin Red S (ARS) was 400 $mg \cdot g^{-1}$. Dinh et al. [41] used UiO-66-NO_2 to adsorb and remove MB and MO. Due to the presence of –NO_2, UiO-66-NO_2 had a strong electronegativity, resulting in a much higher adsorption capacity for MO (142.9 $mg \cdot g^{-1}$) than MB (41.7 $mg \cdot g^{-1}$). Meanwhile, the coexistence of π-π interaction and hydrogen bonding was observed from the adsorption mechanism, but hydrogen bonding played a primary role.

Antibiotics are widely used not only for the treatment or prevention of human and animal diseases, but also to promote animal growth in livestock and aquaculture. Therefore, antibiotics released into the environment seriously endanger the water quality and aquatic organisms. Currently, adsorption removal of antibiotics relies mainly

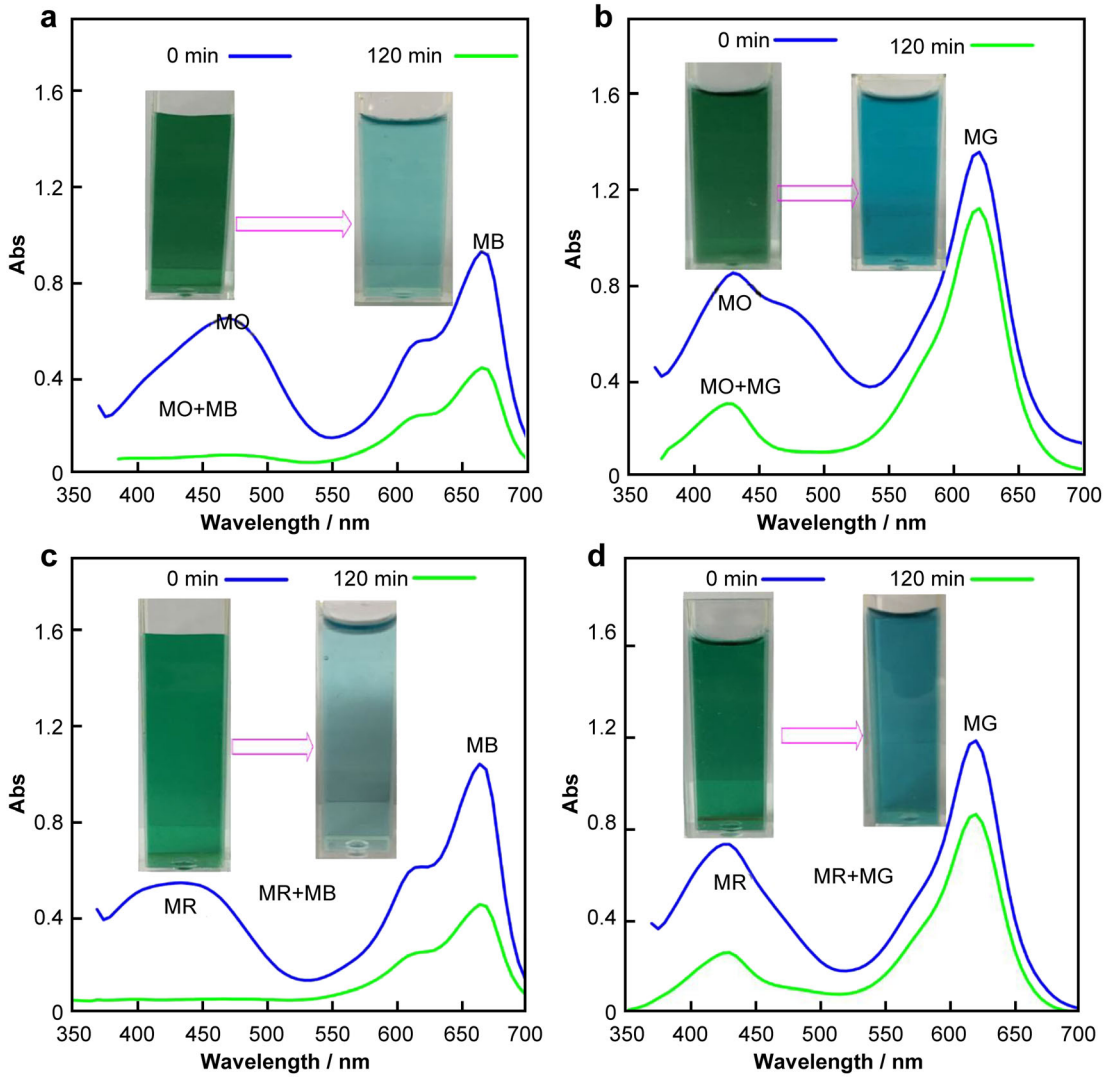

Fig. 2 UV–Vis spectra and adsorption images of different mixtures: **a** MO/MB; **b** MO/MG; **c** MR/MB; **d** MR/MG before and after adsorption onto pristine UiO-66. Reproduced with permission from Ref. [39]. Copyright 2020, Elsevier

on hydrogen bonding, electrostatic interaction, and π-π interaction with material components. Fang et al. [42] used UiO-66-NH_2 for the adsorption of the antibiotic norfloxacin (NOR), and the maximum adsorption capacity was 222.5 mg·g^{-1}. Meanwhile, NaCl and $CaCl_2$ enhanced the removal efficiency of NOR, but humic acid had almost no effect on the adsorption of NOR. The adsorption results showed that when the concentration of NOR was 10 mg·L^{-1}, the removal efficiency of NOR was 91.6%, indicating that UiO-66-NH_2 was suitable for the removal of low concentration antibiotics. Zhuang et al. [43] used UiO-66 and UiO-66-NH_2 for the adsorption removal of diclofenac (DCF). UiO-66-NH_2 had a higher adsorption capacity than UiO-66, with maximum adsorption capacities of 357 and 555 mg·g^{-1}, respectively. The study indicated that the adsorption was an exothermic process, and the adsorption capacity did not change significantly within the pH range of 4.8–7.7. In addition, with the increase of the activation temperature of UiO-66-NH_2, its adsorption capacity for DCF also significantly increased. The adsorption mechanism revealed that hydrogen bonding and electrostatic interaction played an important role in the adsorption of DCF. Liu et al. [44] prepared four functional group Zr-MOFs (UiO-66-H, -NH_2, -NO_2, -Cl) for the adsorption removal of low concentration amoxicillin (AMX), among which UiO-66-NH_2 had the highest adsorption capacity ((2.3 ± 0.4) mg·g^{-1}). Wang et al. [45] prepared UiO-66-$(COOH)_2$/GO composite by combining UiO-66-$(COOH)_2$ and graphene oxide (GO) for the adsorption removal of tetracycline hydrochloride (TC). Compared with pure UiO-66 (27.53 mg·g^{-1}), the adsorption capacity of UiO-66-$(COOH)_2$/GO reached 164.91 mg·g^{-1}, which was attributed to the introduction of GO and -COOH increasing the adsorption sites of

pollutants. The possible mechanism of pollutant adsorption was π-π interaction, chemical coordination, and weak electrostatic interaction (Fig. 3). It can be seen that pure UiO-66 matrix has good adsorption performance for pollutants, but in actual water purification, nano-sized materials are difficult to separate from water and cannot be reused, which affects practical application. Therefore, the preparation of high adsorption capacity and easily separable adsorbents is conducive to the practical application of MOF materials. Li et al. [46] used in-situ composite of polyurethane sponge and UiO-66-NH_2 for the removal of 2,4-dichlorophenoxyacetic acid (2,4-D). Compared with powdered UiO-66-NH_2, the composite material not only maintained the adsorption capacity of 2,4-D, but also was easy to separate. The adsorption result showed that the adsorption capacity of 2,4-D reached 72.99 $mg \cdot g^{-1}$, and the main adsorption mechanism was π-π interaction, as well as hydrogen bonding interaction.

2.2 UiO-66 for heavy metal adsorption

2.2.1 Heavy metal ions

Heavy metals (copper, nickel, mercury, etc.) not only are toxic, but also can accumulate in water bodies, posing a risk to human health through the food chain [47]. Studies have shown that heavy metals are adsorbed and removed primarily by hydrogen bonding, chelation, surface complexation, redox and precipitation. Research indicates that heavy metals can accumulate in apples through their roots, which can then be consumed by humans as fruit juice, further exposing them to health risks [48]. Moreover, industrial and agricultural activities have been identified as sources of heavy metal contamination in water bodies, which can in turn lead to toxicity in organisms and affect the health of migratory birds [49]. In various studies, UiO-66-NH_2 and its modified composites have been used for heavy metal adsorption. Wang et al. [50] used UiO-66-PRAA, modified with phenothiazine-N-rhodanine, to remove Cr(VI) through adsorption. UiO-66-PRAA had a high adsorption capacity of 333.67 $mg \cdot g^{-1}$ at pH = 3 and a temperature of 303 K, and exhibited good cycling performance. The adsorption mechanism was found to be chemisorption, with electrostatic, reduction, and chelation mechanisms operating in that order. Similarly, Tang et al. [51] used UiO-66-PTC, modified with phenylaminothiourea, to adsorb Pb^{2+}, with a maximum adsorption capacity of 200.17 $mg \cdot g^{-1}$. Thermodynamic analysis showed that the adsorption was exothermic and spontaneous, with Pb(II) adsorbed in a monolayer and the rate-controlling step mainly involving chemisorption and chelation with N or S. Yang et al. [48] encapsulated acid-etched UiO-66 in chitosan for the adsorption of Pb(II) and Cd(II), resulting in composites with good structural stability and high adsorption capacities of 654.9 and 343.9 $mg \cdot g^{-1}$, respectively, at 45 °C, due to the presence of −OH and Zr(IV). In a study by Liu et al. [52], UiO-66 was coated with a silicon layer for Cd^{2+} adsorption, resulting in UIO-66@mSi-SO_3H > UIO-66@mSi-SH > UIO-66 in terms of adsorption capacity, with UIO-66@mSi-SO_3H exhibiting the highest capacity of 409.96 $mg \cdot g^{-1}$. Moreover, more than 90% of the adsorbents could be regenerated after 5 cycles. Huang et al. [53] pointed out that Pb(II) was uniformly adsorbed on the

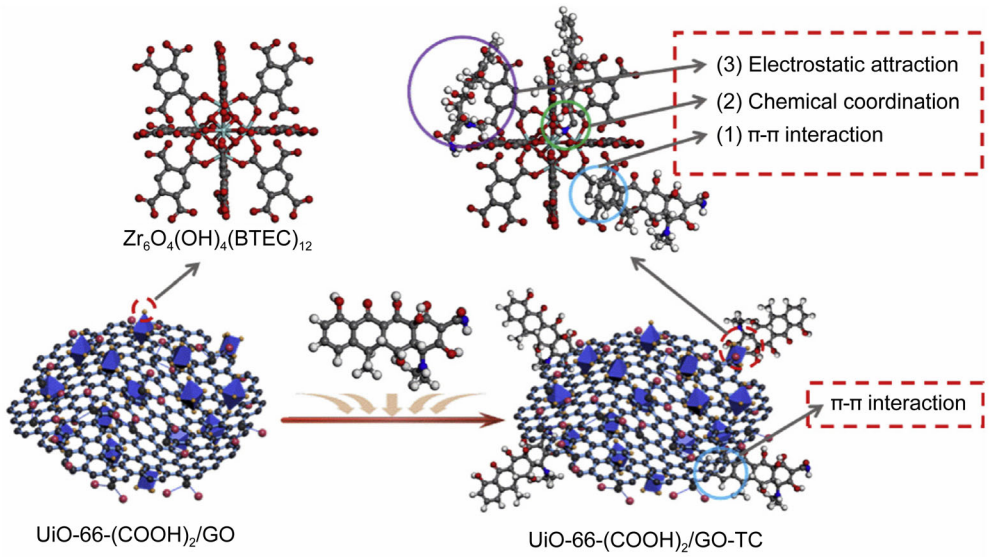

Fig. 3 Proposed mechanisms for adsorption of TC on UiO-66-$(COOH)_2$/GO composites. Reproduced with permission from Ref. [45]. Copyright 2020, Elsevier

surfaces of UiO-66 and UiO-66-NH_2 in the form of a single layer. UiO-66-NH_2 can adsorb 320.73 mg·g^{-1} Pb(II) at 328K and pH = 8. According to Fourier transform infrared spectroscopy (FTIR) (Fig. 4a), the characteristic peak of the material at 1660 cm^{-1} becomes weaker after adsorption, indicating that O in C=O coordinates with Pb^{2+} and the site is occupied by Pb^{2+}. The characteristic peaks of UiO-66-NH_2 at 3360 and 3460 cm^{-1} also become weaker after adsorption, indicating that -NH_2 has strong adsorption performance. In addition, it can be seen from the ion interference experiment that the introduction of -NH_2 promotes the material to have strong stability and ion anti-interference characteristics (Fig. 4b).

2.2.2 Heavy metal ions

Because the use of energy materials such as petroleum and chemical industry has caused pollution of the atmosphere, water and soil, nuclear energy has been rapidly developed. However, the use of nuclear energy inevitably results in the release of radioactive elements (Uranium, Strontium, Cesium, Plutonium, etc.) into the environment [54–56]. Owing to its high chemical toxicity and solubility, even low concentrations will be more harmful to the ecological environment and human health. Researchers typically use adsorption, ion exchange, photocatalysis, biological treatment, and other means to remove radioactive elements. Compared to adsorption technology, these methods can produce more toxic intermediates in the treatment process and cannot be used on a large scale. Zhao et al. [57] investigated the influence of –COOH on the adsorption of U(VI) and Eu(III). The introduction of –COOH reduces the surface charge of UiO-66, resulting in a higher adsorption capacity at low pH. At pH = 3, the adsorption capacity of UiO-66-2COOH for U(VI) and Eu(III) was 100 and 60 mg·g^{-1}, respectively. In order to explore its practical application, it was used in dynamic adsorption experiments, and the results showed that UiO-66-2COOH could adsorb ~ 99% of U(VI)/Eu(III), and could still achieve > 90% adsorption after four cycles. In addition, the adsorption mechanism of elements was investigated by FT-IR. The characteristic peak at 927 cm^{-1} increased significantly after adsorption, indicating that U(VI) was successfully adsorbed on the material (Fig. 5a). The characteristic peak of UiO-66 at 1660 cm^{-1} almost disappeared after the adsorption of U(VI) and Eu(III), indicating that the adsorption of UiO-66 on U(VI) and Eu(III) was a displacement. For UiO-66-COOH and UiO-66-2COOH materials, the missing 1710 cm^{-1} peak is attributed to chemical coordination between adsorbed ions and -COOH (Fig. 5b, c). Meanwhile, Li et al. [58] also used FTIR to investigate the adsorption mechanism of U(VI). After adsorption, the characteristic peak at 908.3 cm^{-1} was classified as the force stretching vibration peak of O=U=O, indicating that U(VI) was successfully adsorbed. In addition, the characteristic peaks at 3424.1, 1432.9, 575.7 and 482.1 cm^{-1} were all shifted, indicating that the amino group and node were the adsorption sites of U(VI) (Fig. 5d). Gumber et al. [59] investigated the adsorption properties of UiO-66(Ce) and CeO_2@UiO-66(Ce) for U(VI) in the pH range of 2–6. Due to the pore blockage of CeO_2, the adsorption capacity of UiO-66 was faster, but the adsorption capacity (190 mg·g^{-1}) was still lower than that of CeO_2@UiO-66(Ce) (239 mg·g^{-1}). In addition, the ion interference experiment shows that the material has good selective adsorption performance for U(VI) in Fe (III), Co (II), Ni (II) and Sr (II) ions.

Adsorption can remove heavy metals and organic pollutants from water under economic conditions, which has been widely concerned. Compared with traditional porous

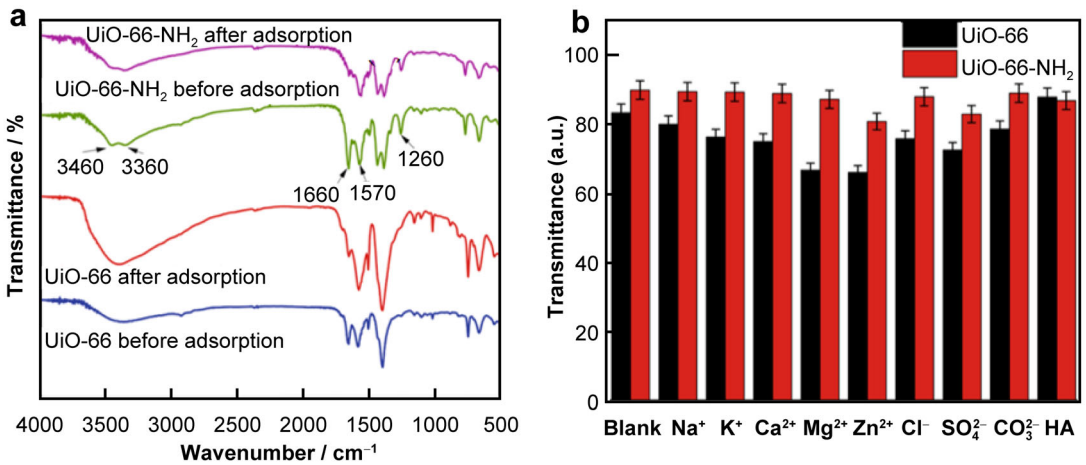

Fig. 4 **a** FTIR spectra of UiO-66 and UiO-66-NH_2 before and after Pb(II) adsorption; **b** effect of various interfering ions and HA on adsorption efficiency. Reproduced with permission from Ref. [53]. Copyright 2022, Elsevier

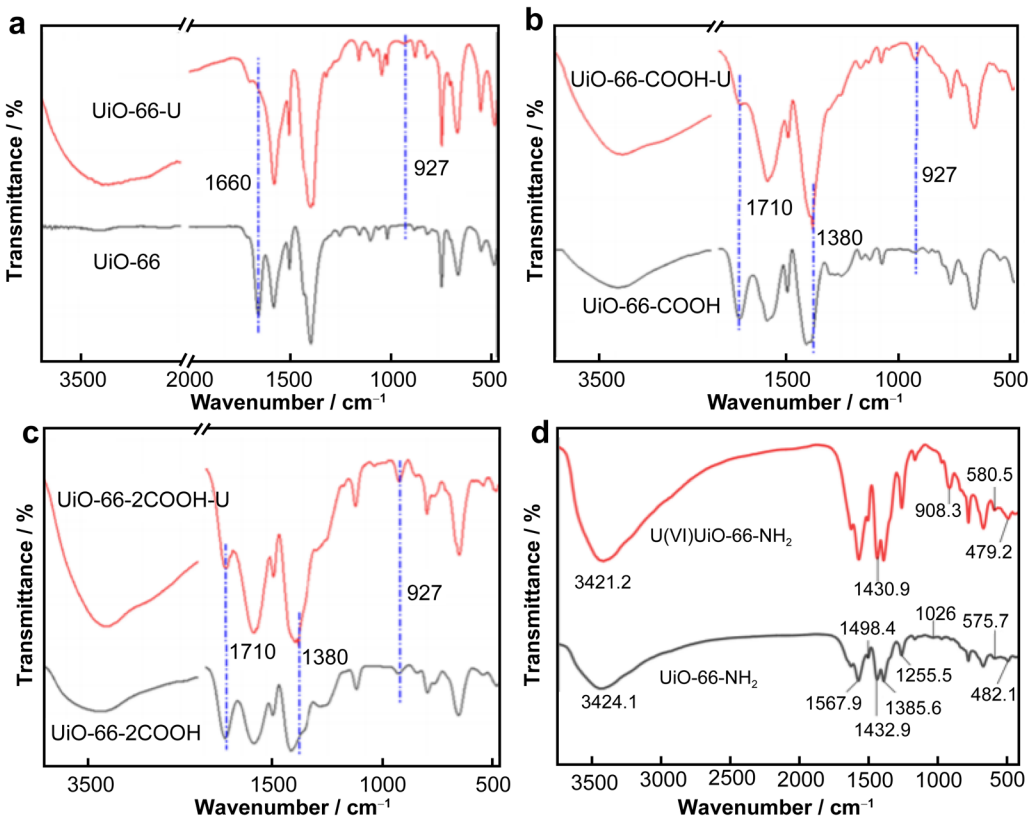

Fig. 5 FTIR spectra of MOFs before (black) and after (red) U(VI) adsorption: **a** UiO-66; **b** UiO-66-COOH; **c** UiO-66-2COOH; **d** FTIR spectra for UiO-66-NH_2 before and after U(VI) adsorption. Reproduced with permission from Ref. [57]. Copyright 2021, American Chemical Society. Reproduced with permission from Ref. [58]. Copyright 2021, Springer

materials, MOFs are more effective at adsorbing and removing pollutants due to their larger specific surface area and high porosity. In addition, exposed metal nodes and ligands of MOF as adsorption sites are also conducive to pollutant removal. Meanwhile, the combination of MOFs with materials containing heteroatoms or metal oxides can increase the absorption of pollutants. Based on the adsorption mechanism, it can be seen that there is not only physical adsorption (pore, cavity size and surface area), but also chemical absorption (surface functionality, surface atomic coordination and electron density) of pollutants.

2.3 UiO-66 for VOC adsorption in gas phase

As a precursor to ozone and $PM_{2.5}$, VOCs are a serious threat to the natural environment and human health, and have been widely studied. Currently, there are many methods for treating VOCs, including combustion, capture, and catalysis [60]. These methods typically have problems with high operating costs, low efficiency, or secondary pollution. In contrast, adsorption can be used to treat VOCs under mild conditions and has the advantages of low cost, simple operation, and no toxic intermediate species [61].

The development of materials with abundant microporous structures is crucial for effective adsorption of VOCs. The mesoporous structure facilitates pollutant transfer while the microporous structure allows for adsorption and enrichment of pollutants. Vo et al. [62] synthesized a large number of UiO-66 materials using a continuous flow tubular reactor under microwave radiation and used them for toluene adsorption. The researchers observed a decrease in toluene adsorption with increasing temperature from 25 to 100 °C, which was attributed to the physical adsorption mechanism of toluene on UiO-66(Zr). At 25 °C, UiO-66(Zr) showed higher toluene adsorption (130 $mg \cdot g^{-1}$) than MOF-5 (32.9 $mg \cdot g^{-1}$), MIL-101(Fe) (98.3 $mg \cdot g^{-1}$), and Zeolite (30.7 $mg \cdot g^{-1}$) under the same conditions. The maximum desorption rate of toluene was nearly 95%. Meanwhile, Vo's group [63] prepared ligand-mixed UiO-66(Zr) materials using the same method and found that toluene adsorption increased with an increase in -NH_2 content. The toluene adsorption increased from 139 to 180 $mg \cdot g^{-1}$ when the -NH_2 content in the ligand increased from 25% to 100%. Recovery of 95% of the toluene adsorbed by each material was achievable.

Vellingiri et al. [64] investigated differences in toluene adsorption among six MOF materials (UiO-66, UiO-

66(NH_2), ZIF-67, MOF-199, MOF-5 and MIL-101(Fe)). The results showed that the saturation adsorption amounts of the six MOFs for toluene were in the order of UiO-66(NH_2) (252 $mg \cdot g^{-1}$) > ZIF-67 (224 $mg \cdot g^{-1}$) > UiO-66 (166 $mg \cdot g^{-1}$) > MOF-199 (159 $mg \cdot g^{-1}$) > MIL-101 (98.3 $mg \cdot g^{-1}$) > MOF-5 (32.9 $mg \cdot g^{-1}$). The authors pointed out that UiO-66 and MIL-101(Fe) were favorable for toluene adsorption due to their large pore or cage structures. The π-bonding force between the uncoordinated metal node Cu of MOF-199 and toluene is also favorable for toluene enrichment. The -NH bonds of UiO-66-NH_2 and ZIF-67 can easily form hydrogen bonds with toluene, giving them relatively high toluene adsorption capacity (Fig. 6).

Hasan et al. [65] used two MOFs, UiO-66 and UiO-66-NH_2, for the adsorption of pyridine in both gas and liquid phases. They showed that the adsorption capacity of UiO-66 for pyridine increased with the proportion of -NH_2 in the ligand, which was attributed to the ability of -NH_2 to form hydrogen bonds with the N atoms in pyridine, facilitating its adsorption.

Zhou et al. [66] prepared a series of UiO-66 materials with different morphological structures by adjusting the content of glacial acetic acid. They observed that the morphological structure of UiO-66 became progressively more regular with increasing glacial acetic acid content, while the specific surface area, micropore volume, and grain size gradually increased. Additionally, when the synthesized material was tested for dichloromethane adsorption at 25 °C and 44 kPa, the adsorption trend was UiO-66–5 > UiO-66–2 > UiO-66-1 > UiO-66-0. The adsorption capacity of UiO-66-5 with a regular morphological structure (510.3 $mg \cdot g^{-1}$) showed a 47.3% increase compared to UiO-66-0 (346.4 $mg \cdot g^{-1}$). Ou et al. [67] also

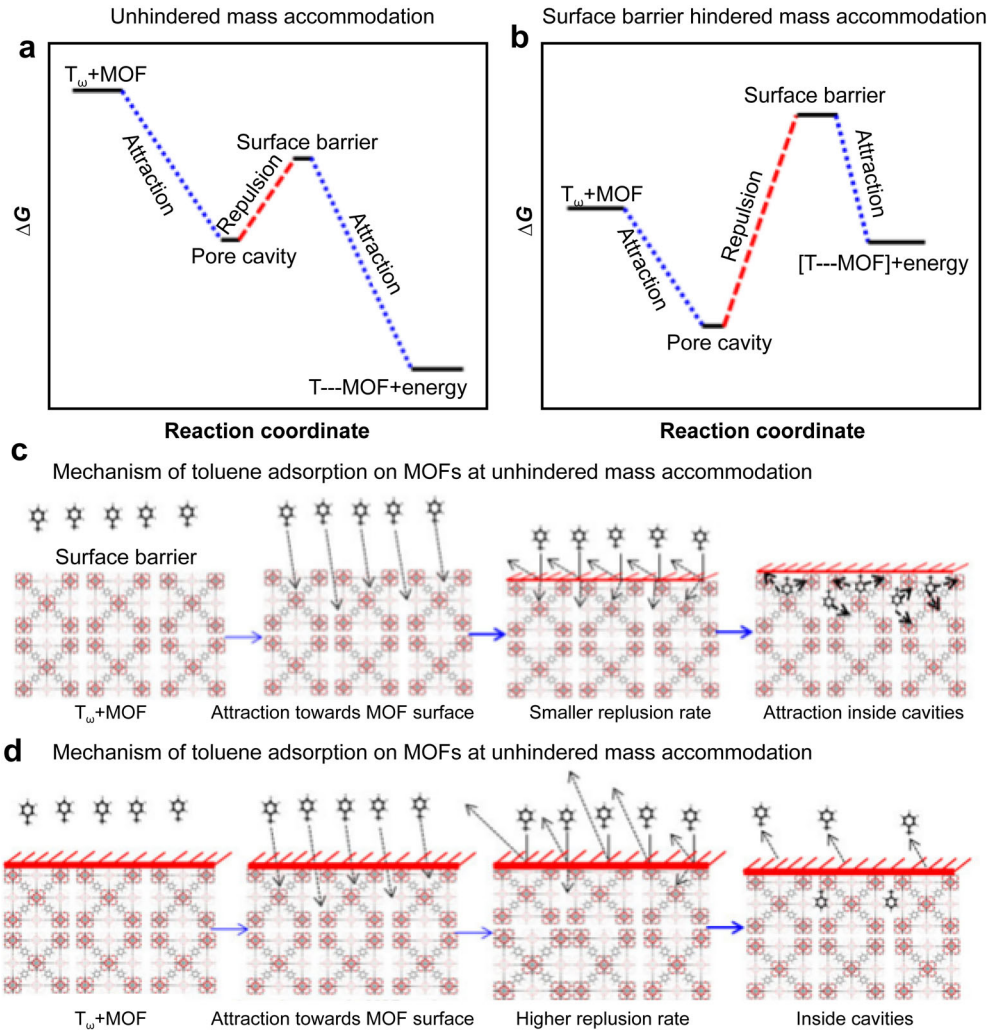

Fig. 6 Schematics of toluene adsorption on MOFs: hypothetical energy profile for gaseous toluene adsorption on MOFs at **a** unhindered, and **b** surface-hindered reactions, **c** and **d** their respective adsorption mechanisms. Reproduced with permission from Ref. [64]. Copyright 2017, Elsevier

prepared a series of UiO-66 with controlled morphology and structural defects for the adsorption of benzene and toluene by adjusting the content of glacial acetic acid. The highest benzene adsorption capacity (367.13 $mg \cdot g^{-1}$) was achieved when the ratio of acetic acid to terephthalic acid was 1 (UiO-66-1.0HAc), resulting in a 49% increase in adsorption capacity compared to UiO-66 without defective sites. Increasing the ratio of glacial acetic acid to terephthalic acid to 2 led to UiO-66-2.0HAc selectively adsorbing a higher capacity of toluene due to the larger diameter and higher polarity of toluene compared to benzene. The toluene adsorption capacity of UiO-66-2.0HAc showed a 93% increase (410.21 $mg \cdot g^{-1}$) compared to UiO-66 without defective sites (Fig. 7).

Zhang et al. [68] modified UiO-66 using cetyltrimethylammonium bromide (CTAB). The results showed that CTAB induced coordination defects in UiO-66, and the resulting defective sites could act as adsorption sites for toluene. Compared to pure UiO-66, the toluene adsorption capacity of UiO-66 modified with CTAB was higher, especially when the molar ratio of CTAB to Zr^{4+} was 0.5, with the highest toluene adsorption capacity (275 $mg \cdot g^{-1}$) achieved. The authors also performed toluene adsorption tests at different temperatures, and the results showed that the toluene adsorption decreased gradually with increasing adsorption temperature (Fig. 8). Additionally, the amount of toluene adsorbed decreased as the relative humidity in the system increased. This was because the hydrogen in H_2O could coordinate with the carboxylic acid in the ligand in the presence of H_2O, which inhibited the adsorption of toluene at the adsorption site. To address the problem of competitive adsorption between toluene and water molecules, this research group [69] used PVP as a structural guide to hydrothermally modify UiO-66 for toluene adsorption. And the results showed that the defective ligand could act as a site for toluene adsorption, where the defective UiO-66 material with PVP/Zr^{4+} of 0.5 had the highest toluene adsorption capacity (259 $mg \cdot g^{-1}$), which was 1.7 times higher than that of pure UiO-66 (151 $mg \cdot g^{-1}$). Especially at a high humidity of 70%, the defective sites of UiO-66 still had 84 $mg \cdot g^{-1}$ of toluene adsorption. Shi et al. [70] synthesized UiO-66-NH_2 with defective sites for the adsorption–desorption of toluene using CTAB as a template agent. Characterization results showed that the defective-site UiO-66-NH_2 exhibited high toluene adsorption due to its high specific surface area, pore capacity and additional adsorption sites caused by the defective sites, with the highest toluene adsorption (228 $mg \cdot g^{-1}$) at a CTAB/Zr^{4+} ratio of 0.5 and little change in the crystal structure of the material before and after adsorption. Importantly, the addition of CTAB impeded the contact between water molecules and hydrophilic groups, which in turn had less effect on the adsorption of toluene by water molecules.

Zhang et al. [71] used MOF-5 as a template to prepare UiO-66 with defective sites for the adsorption of toluene. M-U-0.01 with a MOF-5/Zr^{4+} ratio of 1 had the highest toluene adsorption capacity (257 $mg \cdot g^{-1}$), which was 1.7 times higher than that of the original UiO-66, attributed to the strong interaction between toluene and the defective UiO-66. In addition, the modified UiO-66 exhibited better toluene adsorption properties than the pristine UiO-66, although water molecules and high temperature factors could cause the collapse of the UiO-66 structure, hindering toluene adsorption and reducing the π-π interaction between the material and toluene.

VOCs are organic pollutants and when water molecules are present in the environment, they compete with VOCs for adsorption on the material surface, thus reducing the adsorption capacity of VOCs. Hu et al. [72] used a

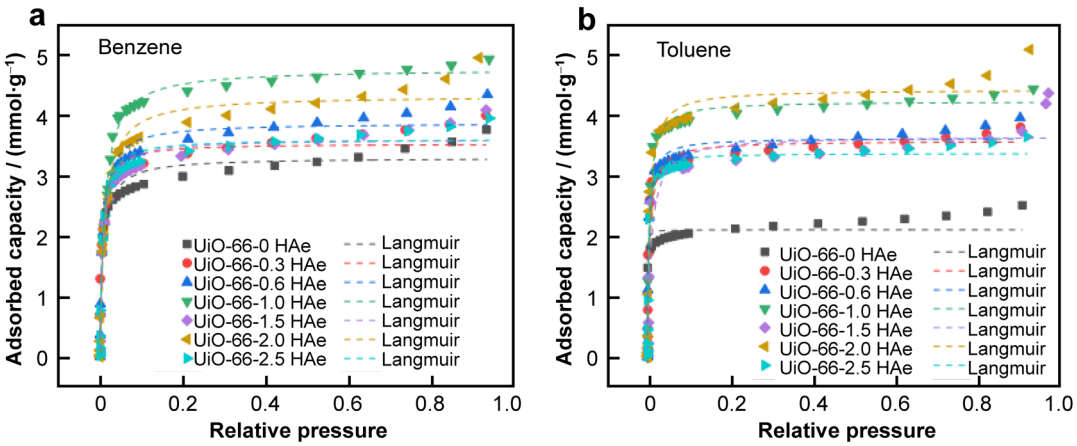

Fig. 7 Adsorption data scatter points of **a** benzene and **b** toluene over BCx-y series adsorbents at different P/P_0 and their tentative fitting isotherms based on Langmuir model simulations at 25 °C. Reproduced with permission from Ref. [67]. Copyright 2021, Elsevier

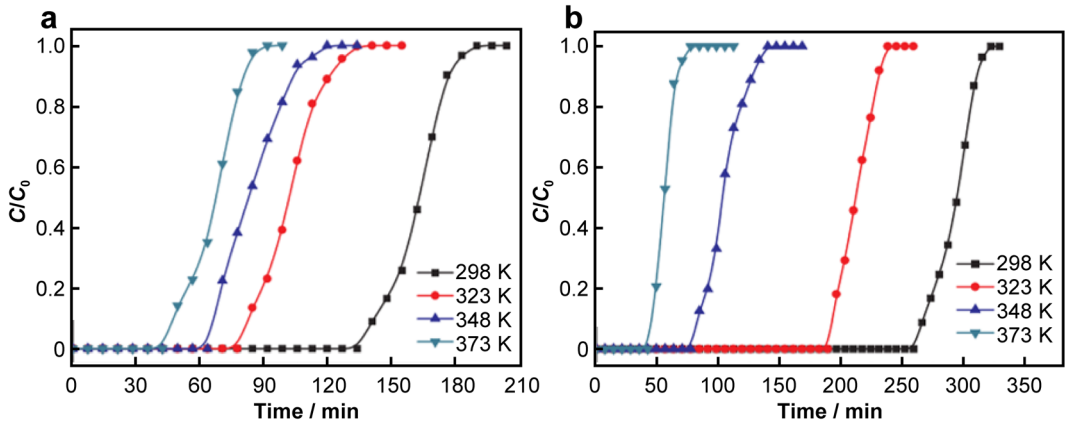

Fig. 8 Breakthrough curves of gaseous toluene on various adsorbents at different adsorption temperatures: **a** UiO-66; **b** CTAB-U-0.5. Reproduced with permission from Ref. [68]. Copyright 2019, Elsevier

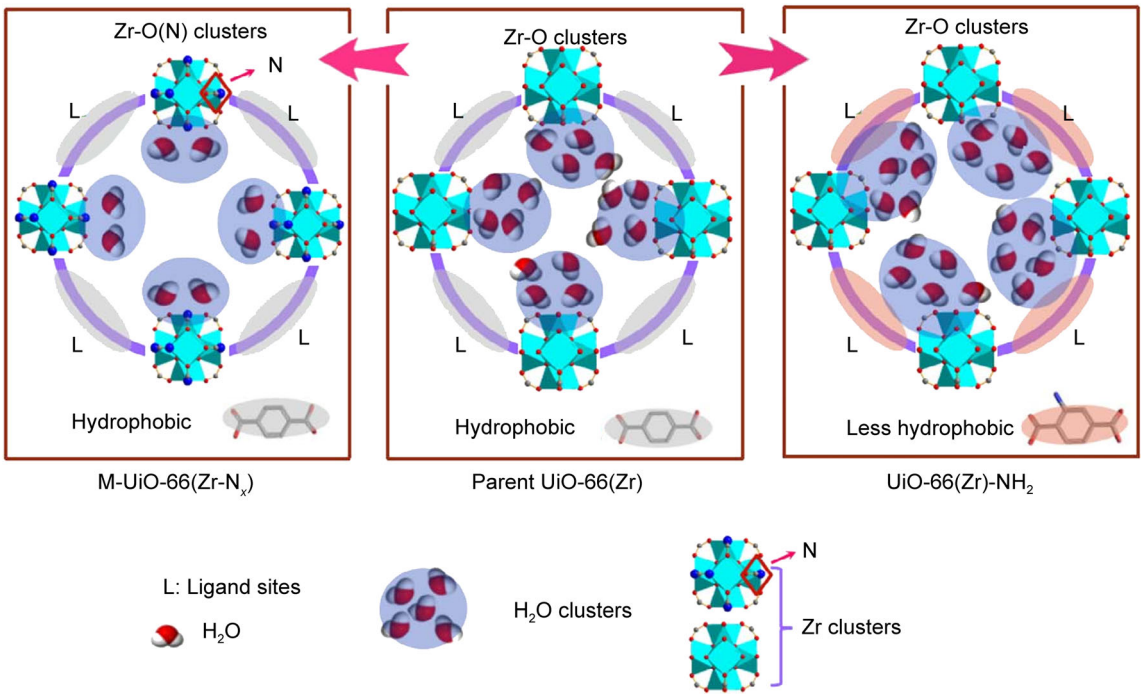

Fig. 9 Bridging effect: water clusters in pores of parent and modified UiO-66(Zr) and resulting voids. Reproduced with permission from Ref. [72]. Copyright 2018, Elsevier

mechanochemical strategy to combine dopamine and UiO-66 to prepare hydrophobic UiO materials for the adsorption of acetaldehyde and chlorobenzene (Fig. 9). Owing to the improved hydrophobic properties of the materials, the N-liganded UiO-66 (labelled as M-UiO-66(Zr-N3.0)) significantly increased the adsorption of acetaldehyde (9.42 $mmol \cdot g^{-1}$) and chlorobenzene (4.94 $mmol \cdot g^{-1}$) compared to UiO-66 and UiO-66-NH_2, while its adsorption of water compared to UiO-66 and UiO-66-NH_2 by 20% and 47%, respectively. In addition, the rate diffusion constants of chlorobenzene on M-UiO-66 (Zr-N3.0) were 7.8 and 40 times higher than those of UiO-66 and UiO-66-NH_2, respectively.

Sun et al. [73] used phenylsilane for the first time to modify metal nodes to obtain UiO-66 with a hydrophobic angle of 161°. The hydrophobised NH_2-UiO-66(Zr)-shp has excellent alkali resistance and is promising for a variety of applications such as organic/water separation, self-cleaning and liquid marble. In addition, UiO-66-NH_2-shp (48.4 μl) adsorbs 12 times more toluene than UiO-66-NH_2 (3.9 μl).

Zhang et al. [74] investigated density functional theory (DFT) calculation for the adsorption of hexaldehydes on MIL-101(Cr), UiO-66, ZIF-8 and Cu-BDC (Fig. 10). The DFT revealed four possible adsorption types: ① C=O in hexal and C–H in UiO-66 ligand (U1); ② C=O in hexal and

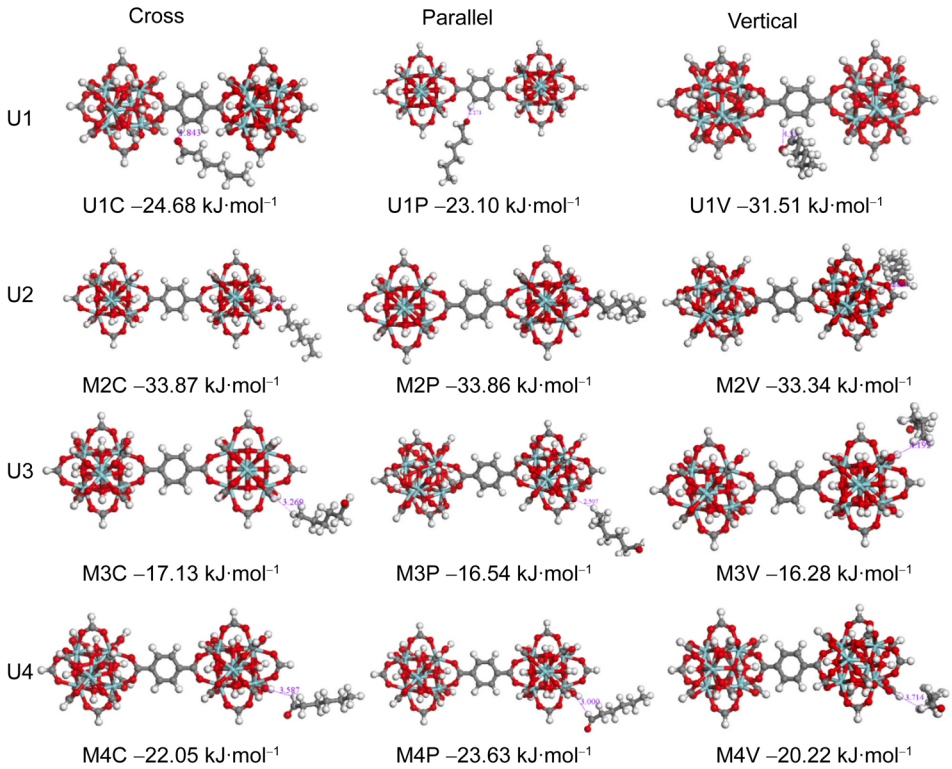

Fig. 10 Optimal configurations obtained via DFT calculations and interaction energy between UiO-66 and hexanal: **a** C–H of linker with C–O in hexanal (U1); **b** Zr–O–H with C-O in hexanal (U2); **c** O–C–O with C–H in hexanal (U3); **d** O–C–O with H in aldehyde group of hexanal (U4). Reproduced with permission from Ref. [74]. Copyright 2020, Elsevier

Zr–OH in UiO-66 (U2); ③ C–H in hexaldehydes and O–C–O in UiO-66 (U3); ④ the aldehyde group of hexaldehydes is H and O–C–O in UiO-6 (U4). U1–U4 play an important role in the adsorption of hexal by UiO-66, and the order of interaction energy is U2 (− 33.34 to − 38.86 kJ·mol^{-1})- > U1 (− 23.10 to − 31.51 kJ·mol^{-1}) > U4 (− 20.22 to − 23.63 kJ·mol^{-1}) > U3 (− 16.28 to − 17.13 kJ·mol^{-1}). The results show that Zr–OH and aromatic C–H in H_2BDC are important adsorption sites for hexanal.

Toluene has been extensively studied as a typical VOC. Compared with traditional molecular sieve and activated carbon, MOF has the advantages of higher adsorption capacity, easy diffusion of VOCs (adjustable pore size structure), selective adsorption of VOCs (benzene ring structure of ligand, hydrophobic modification by grafting) and fast desorption rate. However, VOCs in the atmosphere are not a single entity, but several components coexist. There are many types of VOCs in the atmosphere, which can be divided into alkanes, aromatics, esters, and aldehydes based on their chemical structure. In addition, it can also be divided into polar and non-polar, hydrophilic and hydrophobic. In order to explore the practical application possibility of UiO-66, researchers should pay attention to the synchronous removal of multi-component VOCs, including: the synchronous removal of aromatic-oxygenated VOCs, OVOCs-ClVOCs, aromatic-SVOCs, etc. In addition, water vapor is unavoidable in the real environment, and it is also crucial to explore the selective adsorption of materials.

Based on the above studies, it is clear that UiO-66 based materials can remove harmful pollutants by efficient adsorption under mild conditions, while pollutants with significantly different properties can be selectively adsorbed and have good cycling stability. However, the concentration of pollutants in the real environment is not as high as in the literature and the pollutants in the environment (liquid phase organic pollutants, heavy metals and gas phase VOCs) are not static. It is important that the materials used for the adsorption of pollutants are easily separable from the environment and that the adsorption and removal of pollutants are achieved without adding new sources of pollution. Therefore, it is essential to investigate and obtain UiO-66 based adsorbent materials that can be easily separated and recovered and to achieve the efficient adsorption and removal of pollutants at low concentrations and in dynamic systems.

3 UiO-66 for photocatalytic degradation of organic pollutants

The essence of photocatalysis is that when the energy of incident light is greater than that of the bandgap width, the electron–hole pairs (e^--h^+) generated by the catalytic material are used for the oxidation–reduction reaction of pollutants [75]. Studies have shown that the photogenerated electrons can not only reduce pollutants, but also react with the oxygen adsorbed on the surface of the catalytic material to generate strong oxidizing superoxide radicals ($\cdot O_2^-$). In addition, the h^+ on the valence band can react with H_2O/OH^- on the material surface to generate hydroxyl radicals (·OH) [76]. H^+, O_2^- and ·OH all have strong oxidizing properties, and can selectively oxidize pollutants into harmless CO_2 and H_2O. Therefore, it is crucial to develop an efficient, non-toxic, chemically stable, and easily prepared catalytic material for the photocatalytic removal of pollutants.

3.1 UiO-66 for degradation of liquid phase contaminants

Organic dyes are difficult to decompose in the natural environment and most of them are harmful to both the environment and human health, and can even cause mutations, so dyes must be removed from water. Compared to adsorption techniques, photocatalytic techniques can achieve complete catalytic degradation of pollutants under the action of h^+, ·OH and $\cdot O_2^-$, achieving the goal of harmless treatment. Jin et al. [77] used UiO-66-NH_2, UiO-66-NO_2 and UiO-66-NH_2/UiO-66-NO_2 to photocatalytically degrade RhB, and the results showed that the mixed UiO-66-NH_2/UiO-66-NO_2 had the optimal photocatalytic activity (95.5%) and cyclic stability, and the free radical experiment showed that $\cdot O_2^-$ was the main active species. Mu et al. [78] prepared a series of structurally identical UiO-66 (X = H, NH_2, Br, $(OH)_2$, $(SH)_2$) for photocatalytic degradation of RhB, and the results showed that good visible light absorption did not necessarily mean high photocatalytic activity, but a faster e^--h^+ separation rate and active species generation rate were conducive to rapid degradation of pollutants. Although pure UiO-66 matrix has good pollutant removal rate, there are still problems such as easy carrier recombination and limited light response range. Therefore, researchers generally use semiconductor materials coupled with pure UiO-66 matrix, and the composite material not only has the characteristics of pure MOF large specific surface area and porous structure, but also has excellent photocatalytic properties of semiconductor materials. Bibi et al. [79] prepared a series of BiOBr/UiO-66-NH_2 composite materials using a co-precipitation method for the visible light degradation of the dye RhB. The effective transfer and separation of charges at the heterojunction interface and the synergistic effect of BiOBr/UiO-66-NH_2 resulted in high photocatalytic activity of the composite material, especially for the composite material with 15 wt% UiO-66-NH_2, which could remove 83% of RhB after 2-h light irradiation. Furthermore, the capture experiment showed that h^+ and $\cdot O_2^-$ were the main active species for RhB degradation. Liang et al. [80] prepared core–shell CdS@UiO-66-NH_2 using an in-situ solvothermal method for the degradation of MG and MO. Characterization results showed that the mesoporous UiO-66-NH_2 shell was not only conducive to the absorption of core (CdS) light, but also provided abundant active sites and tightly coupled interfaces between components. The high specific surface area, molecular-level interfacial contact between components, and n–n one-dimensional heterojunction significantly improved the photocatalytic activity of the material, which could remove 99.5% of MG and 95.7% of MO after 25 and 45 min, respectively (Fig. 11). Abdi et al. [81] prepared TiO_2/ZrO_2 composite materials using UiO-66 as a carrier for the degradation of RhB. Owing to the increased absorption of visible light and the rapid separation of charge carriers promoted by the composite material, the composite material had good photocatalytic activity, and after four cycles, it still had high stability and a 90% RhB removal rate.

Antibiotics that are not metabolized in the organism are generally excreted into the environment through forms such as feces and urine, resulting in higher frequencies and concentrations detected in water environments. Yang et al. [82] used UiO-66-NH_2 as a carrier to adjust the morphology of BiOBr for NOR degradation. The 3D structure and tight interface contact of the composite material facilitate the full utilization of light energy, increase the exposure of active sites, and suppress the recombination of carriers. The activity results indicated that the BiOBr/UiO-66-NH_2 composite material with 20% UiO-66-NH_2 had the best photocatalytic activity, and after 180-min illumination, it could remove 93.60% of NOR. The active species capture experiment showed that $\cdot O_2^-$ was the main active species. Cao et al. [83] prepared Co-doped UiO-66 by one-step solvothermal method, and used it for TC adsorption and photocatalytic degradation. The CoUiO-1 composite material with a Zr:Co ratio of 1 had the highest TC adsorption capacity, with an adsorption capacity of 224.1 $mg \cdot g^{-1}$. The high TC adsorption capacity can be attributed to the π-π interaction and electrostatic interaction between the composite material and TC. The adsorbed material can photocatalytically remove 94% of the initial concentration of TC. In addition, the TC adsorption capacity and photocatalytic degradation capacity of CoUiO-1 were 7.6 and 6.9 times that of pure UiO-66, respectively. Wu et al. [30] prepared TiO_2@UiO-66-NH_2 composite material by one-step solvothermal method for TC removal. The composite material had high photocatalytic activity for TC,

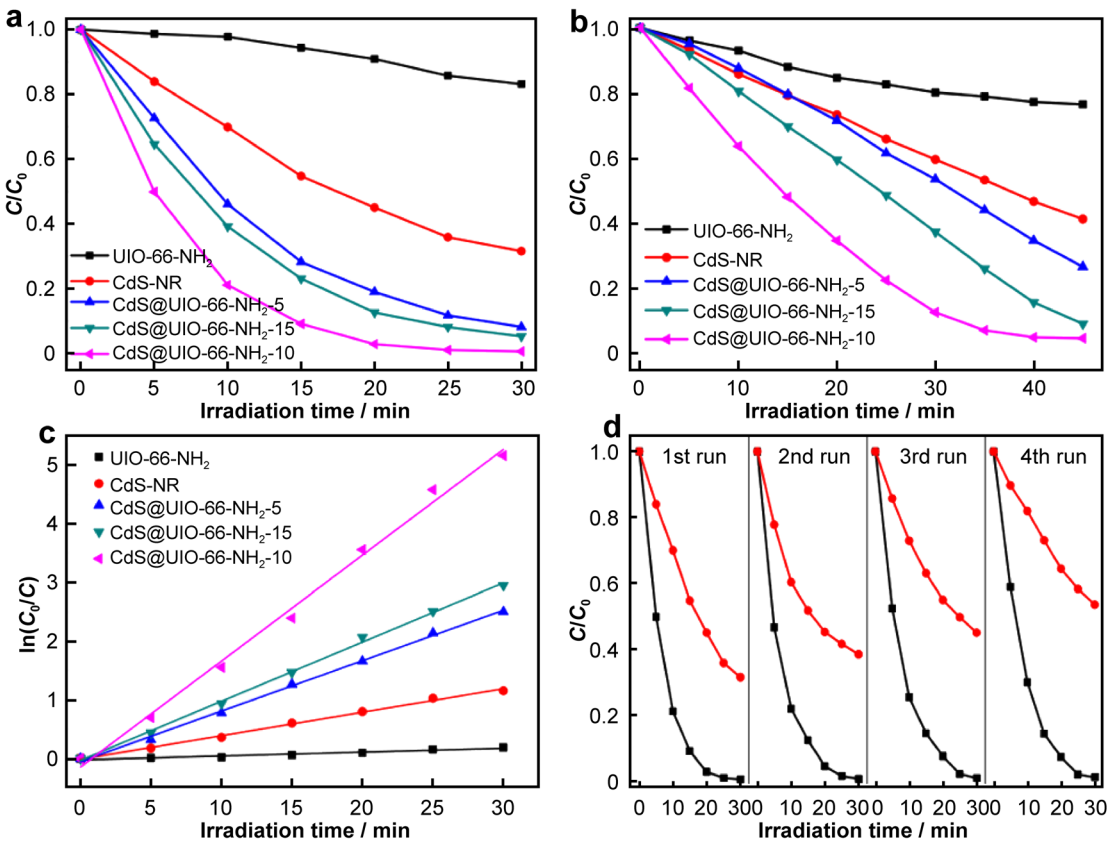

Fig. 11 Photocatalytic degradation of **a** MG, and **b** MO over CdS-NR, UIO-66-NH_2 and CdS@UIO-66-NH_2 composites; **c** the first-order kinetics of MG photocatalytic degradation; **d** photocatalytic recycle degradation of MG over CdS nanorod and CdS@UIO-66-NH_2-10. Reproduced with permission from Ref. [80]. Copyright 2018, Elsevier

which was attributed to its high adsorption capacity for TC and rapid separation of photogenerated carriers. In addition, after four cycles, the photocatalytic activity of the composite material did not decrease significantly, indicating its good stability and recyclability. Zhao et al. [84] used ball milling to prepare Bi_5O_7I/UiO-66-NH_2 for the removal of ciprofloxacin (CIP). Based on the results of active species capture experiments, Schottky tests, electron spin resonance (ESR), and DFT, it was found that the heterojunction of Bi_5O_7I/UiO-66-NH_2 followed a direct Z-type heterojunction electron transfer path. In addition, the characterization results showed that the introduction of UiO-66-NH_2 significantly increased the specific surface area of the material, thereby improving the adsorption capacity for pollutants and the activity sites for degrading pollutants. The activity results showed that the composite material with 50% UiO-66-NH_2 had excellent photocatalytic activity, and after 120-min illumination, it could remove 96.1% of CIP (Fig. 12).

3.2 UiO-66 for reduction of heavy metals

Heavy metal ions produced by processes such as electroplating, tanning, printing and dyeing, polishing, and pigments are widely presented in surface water and groundwater, seriously endangering the natural ecological environment and human health, and have become a pollution problem of global concern [85]. The most common heavy metal ions in water are Cu^{2+}, Cr^{3+}, Ni^{2+}, Pb^{2+}, Hg^{2+} and Cd^{2+}, which are usually removed by photocatalysis, adsorption, membrane separation, and biodegradation methods [86, 87]. Among many methods, photocatalysis is considered an economically effective detoxification method. He et al. [88] encapsulated dye molecules (RhB and Eosin Y (EY)) inside UiO-66 for the reduction of Cr(VI) to Cr(III). Characterization showed that the adsorption capacity of the material for Cr significantly increased after encapsulating the dye molecules, and 99% of Cr(VI) could be removed through adsorption and degradation. After being combined with noble metals, the adsorption capacity of Cr(VI) was significantly reduced due to electrostatic effects, but the reduction efficiency was greatly improved, increasing from 8.4% to 58.2%. Wei et al. [89] used grinding to load a small amount of 3,4,9,10-perylenetetracarboxylic dianhydride (PTCDA) onto the surface of NH_2-UiO-66 for the reduction of heavy metal Cr(VI), and the characterization results showed that the

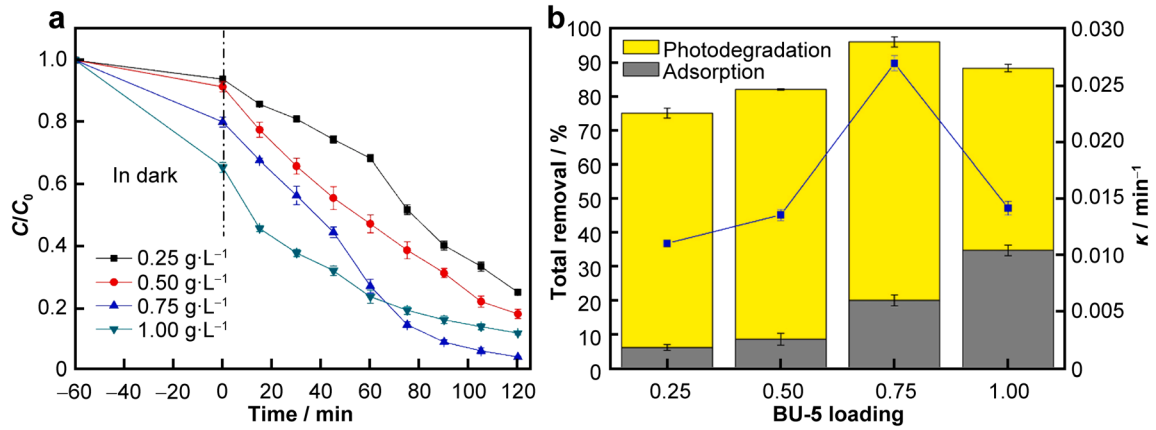

Fig. 12 **a** Adsorption-photocatalytic curves of CIP under different BU-5 loadings; **b** corresponding degree of adsorption, photodegradation and *k* values at conditions of CIP = 10 mg·L^{-1}, pH = 5.8. Reproduced with permission from Ref. [84]. Copyright 2021, Elsevier

addition of PTCDA broadened the material's light absorption range and promoted charge carrier separation for the reduction of Cr(VI). Meanwhile, the activity of the material was explored by changing the pH, initial concentration, and adding small organic acids, among which NU100P10 had the best photocatalytic activity, and still had a good removal rate of Cr(VI) after five cycles. ESR and capture agents showed that e^- and $\cdot O_2^-$ were the main active species for the reduction of Cr(VI). Compared with powdered materials, membrane-type photocatalytic materials have good potential for photocatalytic applications. Du et al. [90] used membrane-type UiO-66-NH_2(Zr/Hf) for the reduction of heavy metal Cr(VI). Owing to the material's good chemical and water stability, it still had a 94% removal rate of Cr(VI) after 20 cycles (Fig. 13).

There are many types of heavy metals in water, and different researchers use different probe molecules to explore the potential applications of UiO-66 material in water remediation. Li et al. [91] used CdS/UiO-66-NH_2 material under non-sacrificial conditions to reduce uranium (VI) in wastewater to trivalent (($(UO_2)O_2{\cdot}2H_2O$) (Fig. 14). The results showed that while e^- and $\cdot O_2^-$ were reducing uranium (VI), h^+ was oxidizing S^{2-} to SO_4^{2-}, and the composite material had a removal rate of 85.62% for uranium-containing wastewater from mines under sunlight.

3.3 UiO-66 for catalytic oxidation of VOCs

Although MOF materials have a large specific surface area, high porosity, and semiconductor properties, their rapid carrier recombination results in poor photocatalytic activity [92]. Therefore, many researchers have synthesized composites of TiO_2 and MOFs, hoping that the composite material can not only maintain the excellent photocatalytic activity of TiO_2 but also inherit the advantages of MOFs' semiconductivity and large specific surface area, thereby overcoming the problems of TiO_2's low adsorption capacity for VOCs and easy carbon deposition deactivation, as well as MOFs' poor activity. Yao et al. [93] synthesized a series of TiO_2@UiO-66-NH_2 materials for the photocatalytic degradation of styrene under visible light dynamic conditions (Fig. 15). Based on the soft-hard acid–base theory, the ultrafine TiO_2 nanoparticles encapsulated that inside UiO-66-NH_2 have good interface contact, and the composite material has good light responsiveness and carrier separation rate. In addition, the 3D structure of UiO-66 facilitates the mass transfer and diffusion of pollutants, forming a VOC-rich environment near the active site. Therefore, compared with pure UiO-66-NH_2 and TiO_2, TiO_2@UiO-66-NH_2 composite materials have excellent styrene removal rate and anti-carbon deposition deactivation performance. TiO_2@UiO-66-NH_2 with 5% TiO_2 can remove 99% of styrene after 600 min of illumination.

Zhang et al. [94] prepared a series of TiO_2-UiO-66-NH_2 composite materials using solvent evaporation method for the photocatalytic oxidation of toluene and acetaldehyde. Due to the higher specific surface area, abundant pore size distribution and intrinsic semiconductor properties of UiO-66-NH_2 compared to traditional porous materials such as activated carbon, TS-1 (Titanium Silicalite-1), and SBA-15 (Santa Barbara Amorphous-15), it exhibited good toluene and acetaldehyde removal rates in the dynamic system. After continuous degradation for 720 min, the removal rate of acetaldehyde and the CO_2 generation of the TiO_2-UiO-66-NH_2 composite material were 10.5 and 14.3 times higher than that of pure UiO-66-NH_2, respectively. Additionally, TiO_2@UiO-66 composite materials were further prepared for the removal of toluene and formaldehyde using a one-step solvothermal method [95]. Characterization of the series revealed that the tight interface contacted

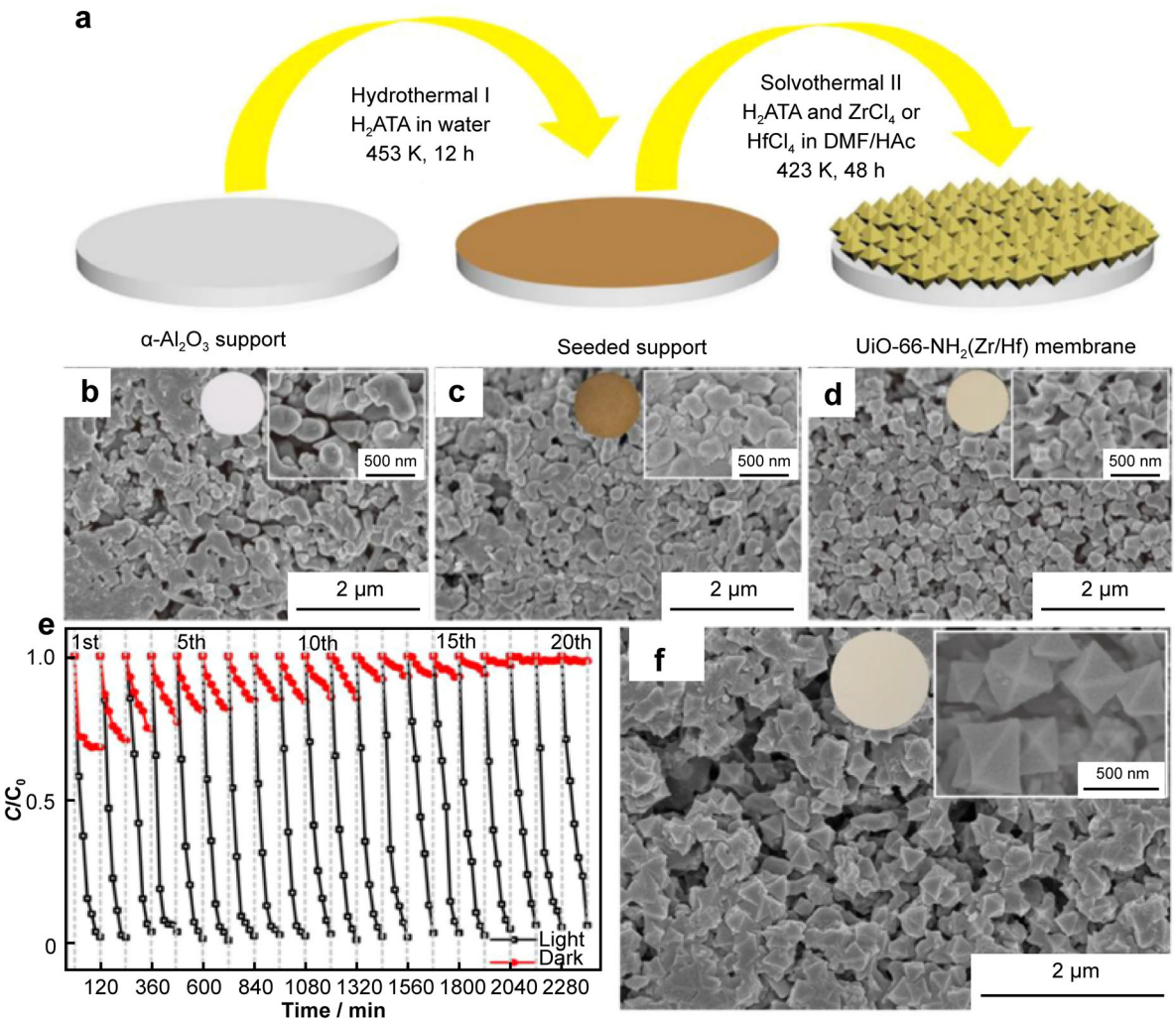

Fig. 13 **a** Schematic diagram of UiO-66-NH_2(Zr/Hf) membrane preparation procedure; SEM images of **b** α-Al_2O_3 support, **c** seed layer, **d** UiO-66-NH_2(Zr) membrane surface and **e** reusability of UiO-66-NH_2(Zr) membrane under simulated sunlight irradiation (photocatalytic Cr(VI) reduction) and at dark conditions (adsorption toward $Cr_2O_7^{2-}$) for 20 successive cycles; **f** SEM image of UiO-66-NH_2(Zr) membrane surface after the 20th photocatalysis experiment. Reproduced with permission from Ref. [90]. Copyright 2019, Elsevier

and matched bandgap structure between components facilitated the rapid separation of charge carriers. Furthermore, UiO-66 preferentially adsorbed toluene and desorbed its degradation product CO_2, which in turn promoted the deep catalytic oxidation of toluene and avoided carbon deposition deactivation of the material. Most importantly, the degradation pathway of toluene was investigated by in-situ infrared spectroscopy, which showed that toluene was first degraded to benzaldehyde and benzoic acid, and then opened to form small molecule oxalic acid, ultimately degrading to harmless CO_2 and H_2O (Fig. 16).

3.4 UiO-66 removing compound contamination

Due to the discharge of industrial, agricultural, and municipal wastewater, water bodies are contaminated with heavy metals such as Cd, Cr, Ni and Pb to varying degrees [96, 97]. The wastewater discharged from industries such as petroleum, coal mining, metal smelting, and tanning also contains serious complex pollution of heavy metals and organic pollutants [98, 99]. Therefore, it is known that pollutants in water bodies do not exist in a single form, but in multiple forms of coexisting pollution. Photocatalytic technology can use the electron–hole pairs generated by the material itself for the reduction of heavy metals and the oxidation of organic pollutants, and thus, it is considered a green and feasible treatment technology. Zeng et al. [100] used Ag_2CO_3@UiO-66-NH_2/GO membrane under flow conditions for the removal of liquid-phase organic pollutants and the reduction of heavy metal Cr. The study showed that the composite material could completely remove MB, RB and MR under the condition of

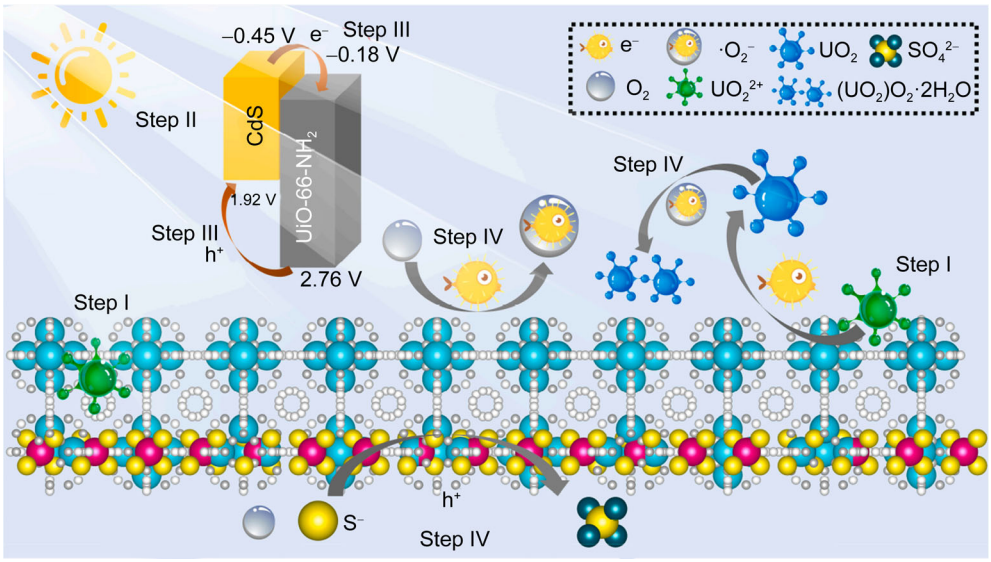

Fig. 14 Proposed mechanism for photocatalytic reduction uranium by 40%CdS/UiO-66-NH_2 under visible-light illumination. Reproduced with permission from Ref. [91]. Copyright 2022, Elsevier

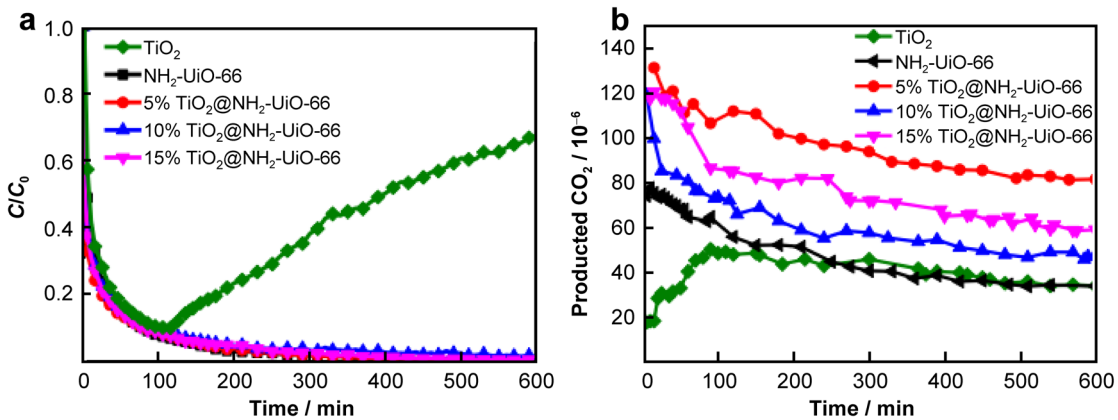

Fig. 15 Evolution of **a** styrene and **b** formed CO_2 during direct photocatalytic oxidation reaction by TiO_2, NH_2-UiO-66 and TiO_2@NH_2-UiO-66 composites. Reproduced with permission from Ref. [93]. Copyright 2018, Elsevier

50 $L{\cdot}m^{-2}{\cdot}h^{-1}$. In addition, after a long time experiment of 200 min, the AgCO@UiO/GO membrane maintained a high removal rate for all dyes and Cr(VI) under light conditions. Zhou et al. [101] prepared a series of UiO-66-NH_2/Ag_2CO_3 composite materials for the reduction of heavy metal Cr and the oxidation of organic pollutants (RhB, MO, CR and MB) using ion exchange method. The authors pointed out that the composite material (marked as UAC-100) had the optimal photocatalytic activity when the mass ratio of UiO-66-NH_2 to Ag_2CO_3 was 1:1. Cr can be completely reduced in 50 min, 96% of MB and 81% of CR can be degraded after 60 min, and 90% of MO and 85% of RhB can be degraded after 90 min. In addition, after four cycles, it still maintained a 99% removal rate for Cr (Fig. 17).

Environmental pollution and energy consumption are two major problems facing society. The simultaneous removal of pollutants and energy generation has attracted attention. Based on the redox properties of photo-generated e^--h^+ pairs, researchers have achieved simultaneous pollutant degradation and hydrogen production. Zhao et al. [102] prepared a series of NH_2-UiO-66/$ZnIn_2S_4$ composite materials using a hydrothermal method for the degradation of MG and hydrogen production. Characterization results showed that the II heterojunction formed by the composite material broadened the spectral response range, promoted the separation of charge carriers, and thereby increased the lifetime of photo-generated charges. The activity results showed that the composite material with 10% NH_2-UiO-66 (10% NU66/ZIS) had a 98% MG removal rate and a

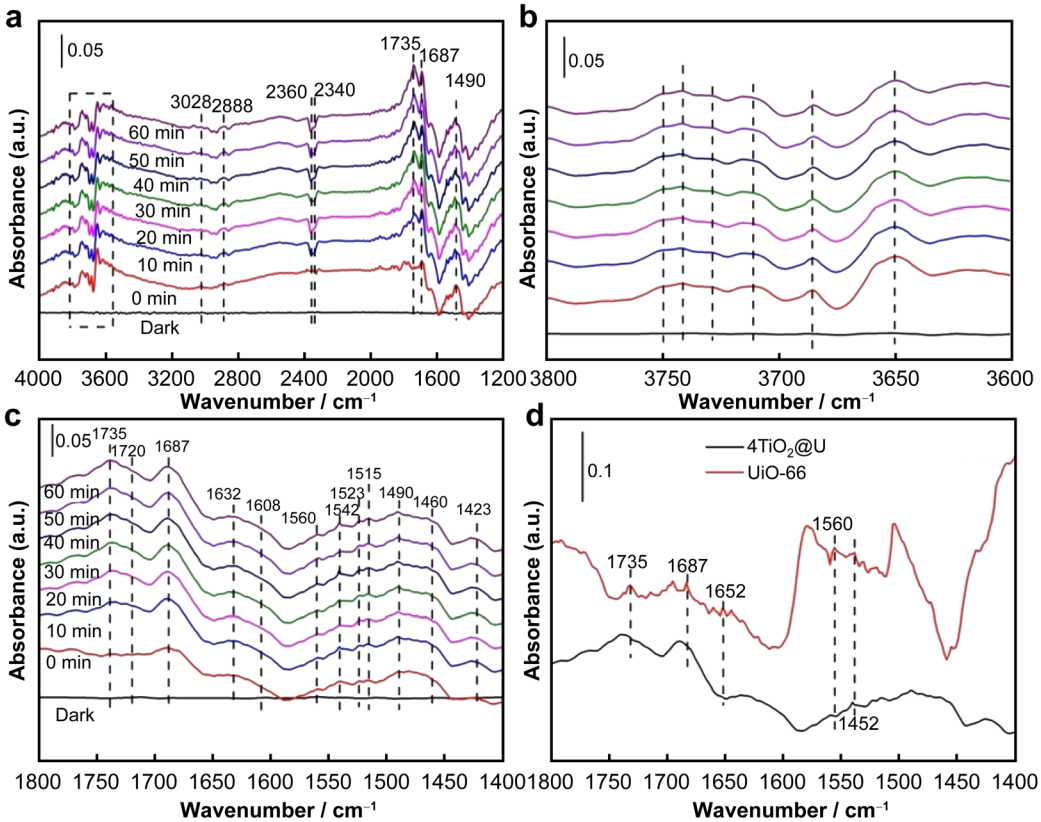

Fig. 16 In-situ FTIR spectra of toluene oxidation **a** on $4TiO_2$@U, **b**, **c** at wavenumber range of 3800–3600 and 1800–1400 cm^{-1} from Fig. 15a, and **d** on UiO-66 and $4TiO_2$@U at 60 min under UV light irradiation. Reproduced with permission from Ref. [95]. Copyright 2021, Wiley

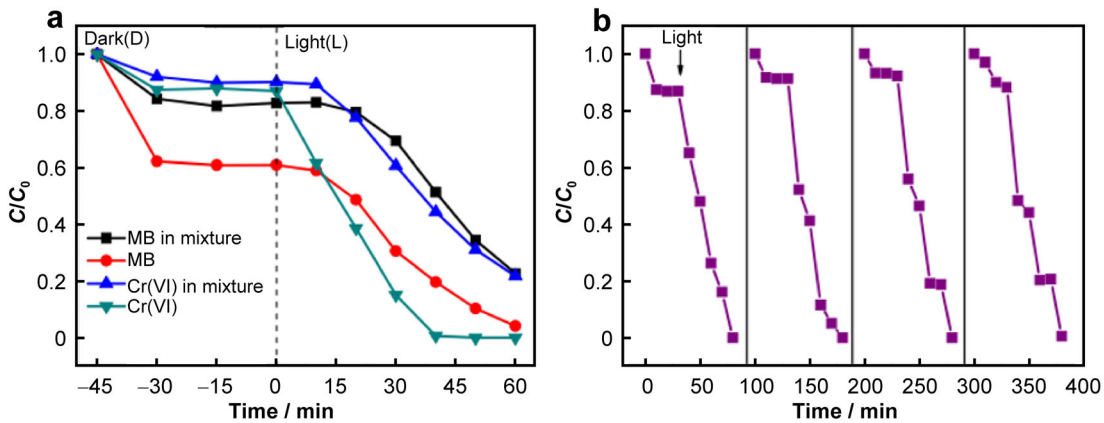

Fig. 17 **a** Photocatalytic Cr(VI) reduction and MB degradation efficiencies in their single systems and in their matrix with UAC-100 as photocatalyst; **b** reusability of UAC-100 under visible light conditions (photocatalytic reduction of Cr(VI)) and dark conditions (adsorption of $Cr_2O_7^{2-}$). Reproduced with permission from Ref. [101]. Copyright 2019, Elsevier

hydrogen production rate of 2199 $\mu mol \cdot h^{-1} \cdot g^{-1}$ (Fig. 18). The use of electron reduction of heavy metals/H_2 production and hole oxidation of organic pollutants can not only avoid carrier recombination, but also realize economic removal of pollutants. Therefore, photocatalysis can be considered as a green pollutant removal technology with high application potential.

Based on the above results, it can be seen that although MOF has received extensive attention as a semiconductor material, its weak electron–hole formation ability leads to its poor catalytic activity. Therefore, researchers generally use the introduction of electron-withdrawing groups, electron-donating groups, or bonding with semiconductor materials to improve photocatalytic activity. The large

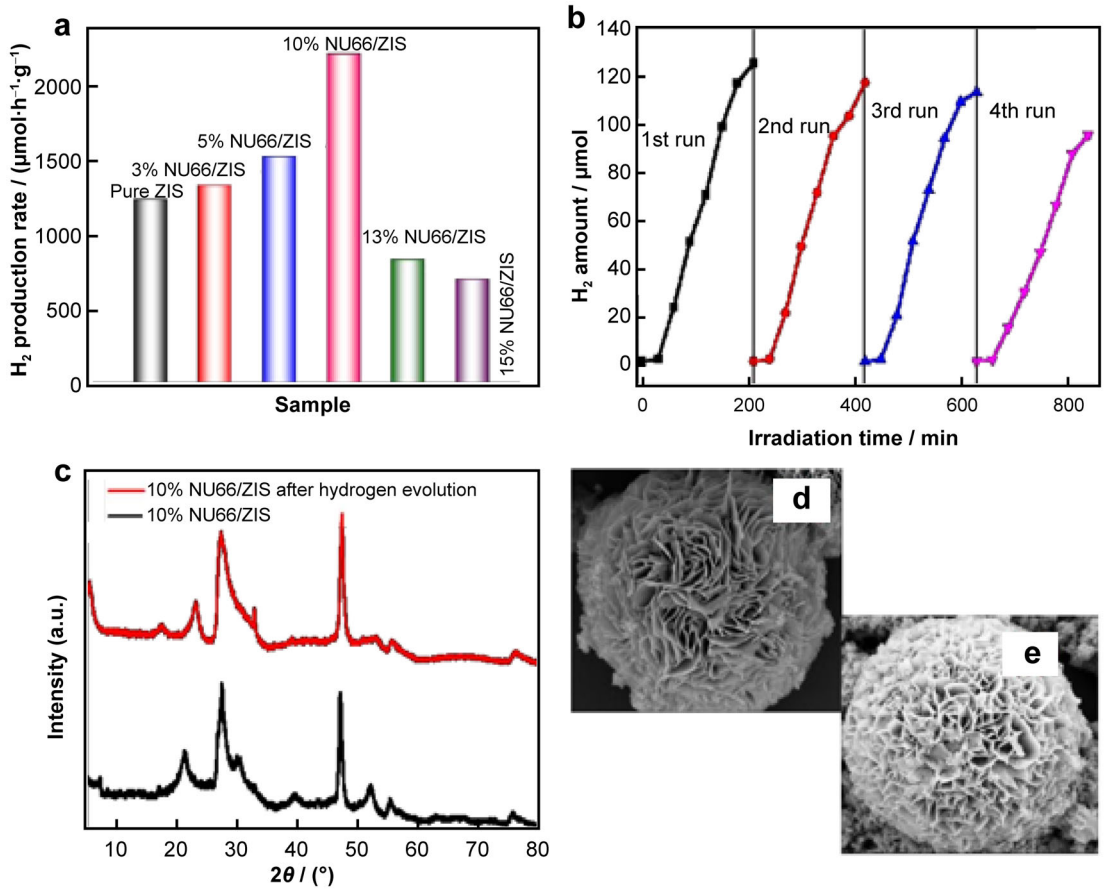

Fig. 18 **a** Photocatalytic H_2 evolution amount of pure ZIS, NU66 and NU66/ZIS composites; **b** cyclic H_2 evolution curves of 10% NU66/ZIS composite; **c** XRD patterns of 10% NU66/ZIS composite before and after cyclic H_2 evolution curves; FESEM images of 10% NU66/ZIS composite **d** before and **e** after cyclic H_2 evolution curves. Reproduced with permission from Ref. [102]. Copyright 2019, American Chemical Society

surface area of the composite material is conducive to the dispersion of active sites, which in turn facilitates the contact between the photoexcited active sites and the pollutants, achieving efficient degradation of pollutants. Meanwhile, the composite material inherits the porous properties of the UiO-66 substrate, which promotes rapid mass transfer of pollutants while realizing rapid separation and transfer of charge carriers to active sites for pollutant degradation. In addition, the close contact and synergistic effect between the components of the composite material promote the transfer of charge carriers and the generation of a large number of active oxygen species, thereby completely mineralizing and oxidizing pollutants.

4 UiO-66 for photocatalytic H_2 and CO_2 reduction

As a practitioner of ecological civilization and an active participant in global climate governance, China has proposed the goal of "Peak Carbon Dioxide Emissions" and "Carbon Neutrality" as it embarks on the journey of the 14th Five-Year Plan. It explicitly requires all regions to urgently develop action plans to peak carbon emissions before 2030 and supports those with conditions to take the lead in achieving this goal, incorporating it into the overall layout of China's ecological civilization construction. Solar energy, as a clean and renewable energy source, can convert solar energy into chemical energy, providing alternative solutions to environmental and natural resource problems.

4.1 UiO-66 removing compound contamination

As an important material foundation for the development of modern society, clean energy has a direct impact on social and economic development and the survival of human society. From the perspective of green chemistry, photocatalytic hydrogen production technology is an ideal strategy for supplying hydrogen energy and reducing the energy consumption of the chemical industry, and the development of efficient and stable photocatalysts is key to the development of hydrogen production technology. Cao

et al. [103] used flower-like Pd@UiO-66-NH_2@$ZnIn_2S_4$ to produce hydrogen under visible light. The composite material has good hydrogen production activity due to its matched bandgap structure, wide spectral response range, and rapid separation of charge carriers. 0.3% Pd@UiO-66-NH_2@$ZnIn_2S_4$ has the best hydrogen production rate (5.26 mmol·g^{-1}·h^{-1}), which is 17 times and 3.8 times the yield of pure $ZnIn_2S_4$ and UiO-66-NH_2/$ZnIn_2S_4$, respectively. At the same time, the quantum yields of 0.3% Pd@UiO-66-NH_2@$ZnIn_2S_4$ at 320 and 420 nm are 20.4% and 3.2%, respectively. Wei et al. [104] synthesized n-p-n type α-$SnWO_4$/UiO-66(NH_2)/g-C_3N_4 material by solvothermal method for hydrogen production and ibuprofen degradation. Due to the double heterojunction promoting the separation of charge carriers and the synergistic effect between the components, the photocatalytic hydrogen production efficiency of the composite material is 2105 μmol·g^{-1}·h^{-1}, which is 21 times that of α-SW (105 μmol·g^{-1}·h^{-1}) (Fig. 19). Shi et al. [105] prepared UiO-66-NH_2 composite material sensitized by auramine O by hydrothermal method. Due to the bidentate coordination between the components, the hydrogen production rate of the hydrothermally sensitized material is 8 times that of the room temperature sensitized material. At the same time, the apparent quantum efficiency of the material at 500 nm is 17.6%. Tian et al. [106] constructed Ti_3C_2/TiO_2/UiO-66-NH_2 for photocatalytic hydrogen production for the first time. Due to the synergistic effect between the components, the separation rate of charge carriers is increased. In addition, due to the excellent conductivity of Ti_3C_2 and the good dispersibility of UiO-66-NH_2 in the composite material, more active sites are exposed, resulting in a hydrogen production rate that is 2.1 times that of UiO-66-NH_2. Sun et al. [107] first encapsulated single-dispersed, small particle size, and non-noble metal phosphides (TMPs, such as Ni_2P and $Ni_{12}P_5$) inside UiO-66-NH_2 for photocatalytic hydrogen production. Compared with pure UiO-66-NH_2 and physically mixed composite materials, the phosphide-encapsulated material (TMPs@MOF) has the best hydrogen production activity. At the same time, kinetics and thermodynamics show that TMPs and Pt have similar properties, which is conducive to the separation of charge carriers and the reduction of the activation energy for H_2 generation.

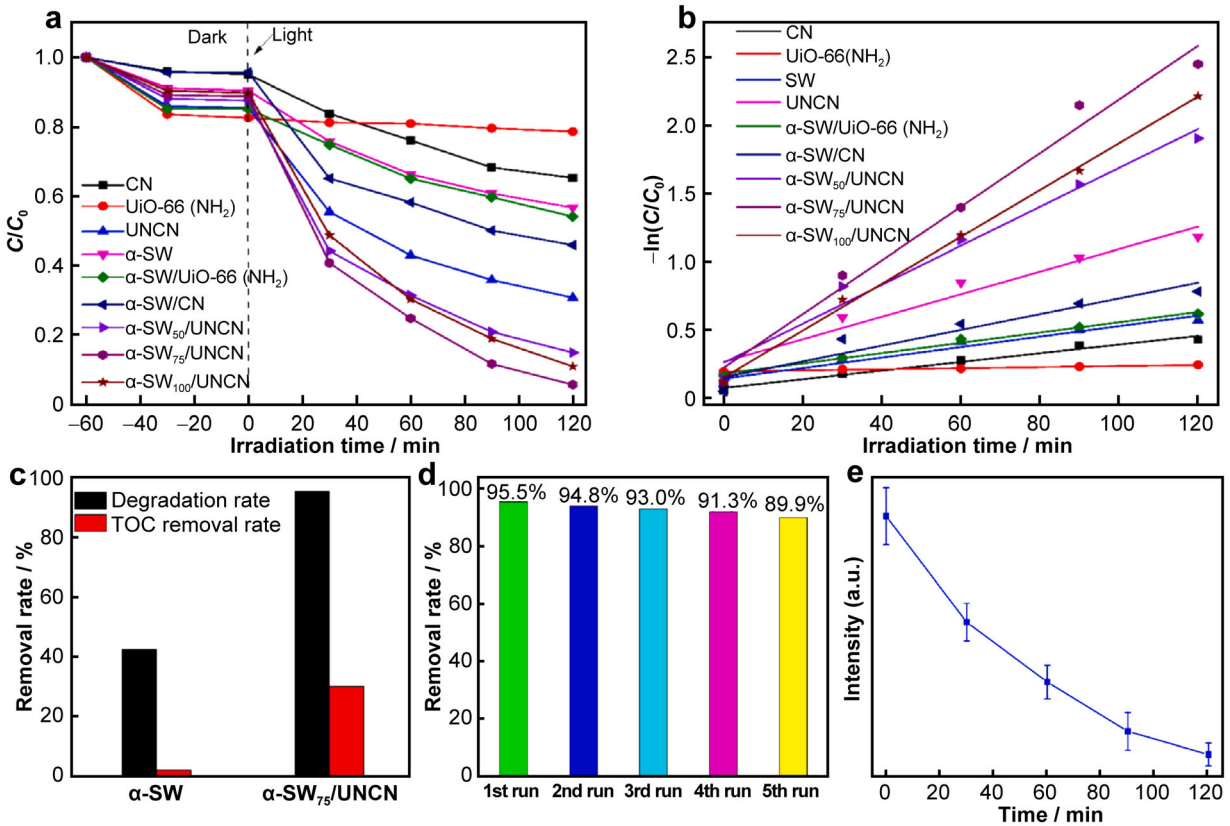

Fig. 19 **a** C/C_0 of IPF solution changes with time in various samples; **b** photodegradation kinetics of IPF by means of plotting ln(C_0/C) versus time; **c** TOC removal rate, and **d** recycle experiments of photodegrading IPF over α-SW75/UNCN; **e** fluctuation of photocatalytic degradation reaction process at different time. Reproduced with permission from Ref. [103]. Copyright 2021, Elsevier

4.2 Photocatalytic CO_2 reduction

Due to the combustion of fossil fuels, CO_2 content in the atmosphere has significantly increased. The problems of ocean acidification and global warming caused by CO_2 have attracted widespread attention from society. Currently, various strategies are being used for CO_2 separation and capture, such as wet scrubbing and dry adsorption [108]. CO_2, as a source material rich in C1, can be converted into various high-value-added products. From a green and sustainable perspective, using clean solar energy to catalyze the resource utilization of CO_2 is an ideal CO_2 management technology, which not only solves environmental problems but also produces energy materials [109, 110]. Wang et al. [110–112] used Cu atomic composite Cu SAs/UiO-66-NH_2 for CO_2 reduction. Due to the promotion of Cu SAs in the conversion of CO_2 to intermediate species CHO* and CO*, the material has high methanol and ethanol yields of 5.33 and 4.22 $\mu mol \cdot h^{-1} \cdot g^{-1}$, respectively. Wan et al. [111] used $CsPbBr_3$ quantum dots and UiO-66-NH_2 composites for CO_2 reduction. Due to the material's large specific surface area, good visible light adsorption capacity, and rapid separation and transfer of carriers, it has a CO yield of 98.57 $\mu mol \cdot g^{-1}$. In addition, CO and CH_4 can be detected simultaneously by gas chromatography, but H_2 cannot be detected. Furthermore, the material has good cycling stability and thermal stability (Fig. 20). Wang et al. [112] used Au nanoparticles (Au-NPs) and reduced graphene oxide (GR) co-modified UiO-66-NH_2 for CO_2 reduction. Based on the plasmonic effect of Au-NPs and the conductivity and large specific surface area of GR, Au/UiO-66-NH_2/GR material has high photocatalytic activity (49.9 μmol) and selectivity (80.9%). Zhao et al. [113] pointed out that UiO-66-NH_2/RGO with covalent bonds had a good CO yield, mainly because covalent bonds facilitate the rapid separation of carriers, which are used for CO_2 adsorption on the surface of RGO. Hu et al. [114] used $NaBH_4$ reduction method to prepare UiO-66-NH_2 composite material with active center Co for CO_2 reduction. Co not only promotes electron transfer but also acts as an active center, making its CO yield 10.2 times that of UiO-66-NH_2. Wang et al. [112] synthesized UIO-66-NH_2/CNTs for CO_2 photocatalytic reduction by hydrothermal method. Carbon nanotubes (CNTs) can promote the conductivity of the material and the dispersion of UiO-66-NH_2, exposing more active sites of the material and promoting CO_2 adsorption and selective generation of HCOOH (63.1%).

5 Hazards of environmental pollutants to humans

With the rapid development of the economy, people's demands for the surrounding living environment and their own living conditions are increasingly high. Therefore, various decoration materials are used for environmental beautification and a variety of clothing and dyes are used for daily life. Research has shown that humans spend about 80% of their time indoors, especially the elderly and children. Pollutants such as benzene and aldehydes released from indoor decoration materials seriously endanger human health and cause harm such as childhood asthma, neurological diseases, and blood diseases [109, 115, 116]. Regarding substances such as clothing and dyes, they not only cause chemical pollution of water bodies by dyes and other chemicals but also cause serious problems such as allergies, miscarriages, and premature births in pregnant women [117]. At present, researchers in the medical and environmental fields are concerned about these pollutants from the aspects of harm to the human body and purification. Environmental researchers typically use a variety of methods to prepare different materials for contaminant removal (the concentration of pollutants in the simulated experiment is much higher than that in the real environment). After adsorption or catalysis, 88.5%–99.6% of pollutants can be removed [57, 79–82, 88, 93–95]. Medical researchers are mainly concerned with the damage to the environment and the human body caused by low concentrations of pollutants in the real environment. Although both have made some research progress and achieved a series of significant research results, there is no substantial mutual guidance between the two fields, such as the selection of pollutant concentration in the environmental field, the cycle of self-degradation of pollutants, the harm of multi-component pollutants, the difficulty of degradation of multi-component pollutants, and the influencing factors of degradation of low-concentration pollutants. In view of this, based on the research results in the field of environment, this section examines the damage to the environment and human body caused by unremoved 12%–1% pollutants in the environment [57, 79–82, 88, 93–95].

5.1 Effects of water pollution on human health

Water is a vital and limited resource for the survival of living organisms, so ensuring the safety of water bodies is crucial. Studies have shown that dozens of antibiotic organic pollutants exist in the seven major river basins in China, including the Yellow River, Yangtze River, Haihe River, Songhua River and Pearl River. In addition, different concentrations of antibiotic substances have been detected in urban sewage discharge [118–120]. These antibiotic pollutants enter water bodies mainly through the production and consumption process, which not only cause malformation of embryos or young children, but also some substances have carcinogenic, teratogenic and mutagenic effects, seriously endangering human health [121–123].

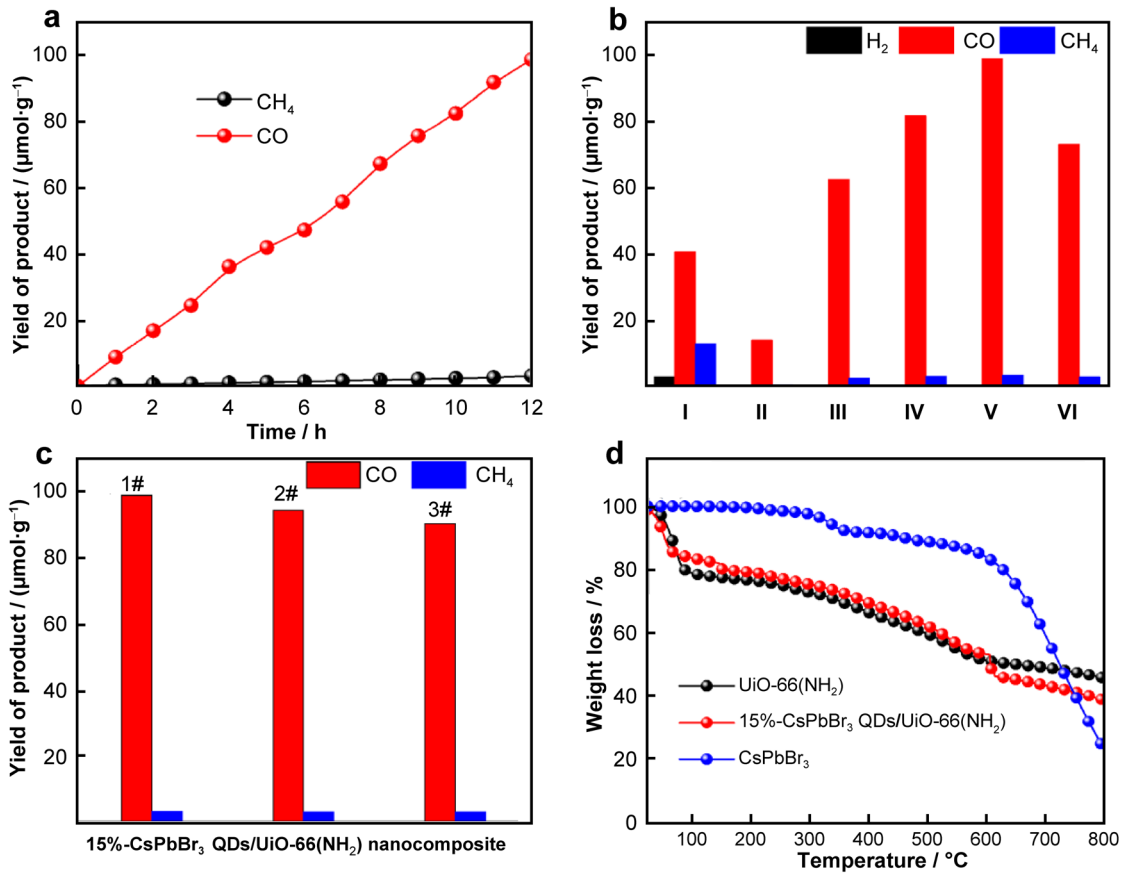

Fig. 20 **a** Photocatalytic CO_2 reduction into chemical fuels under 300-W Xe lamp for 15%-$CsPbBr_3$ QDs/UiO-66(NH_2); **b** photocatalytic CO_2 reduction performance for $CsPbBr_3$ QDs (I) and *x*%-$CsPbBr_3$ QDs/UiO-66(NH_2) nanocomposite (II–VI, *x* = 0, 5, 10, 15, 30); **c** reusability of 15%-$CsPbBr_3$ QDs/UiO-66 (NH_2) nanocomposite; **d** TGA curves of $CsPbBr_3$ QDs, UiO-66 (NH_2) and 15%-$CsPbBr_3$ QDs/UiO-66(NH_2) nanocomposite. Reproduced with permission from Ref. [29]. Copyright 2019, Elsevier

Research has shown that antibiotics accumulate in aquatic organisms such as fish, shrimp, and crabs, and their antibiotic-resistant bacteria and resistance genes can pose a potential threat to human health [124] (Fig. 21). Organic dyes can not only accumulate in fish and cause carcinogenic, teratogenic and mutagenic effects in organisms, but can also lead to significantly higher levels of heavy metals in algae in dye wastewater [125]. About 60% of water is used for crop irrigation, leading to a significant increase in the concentration of pollutants in surface water/groundwater or soil moisture layers. Therefore, the quality of irrigation water is crucial for living organisms [126]. Muhammad et al. [127] pointed out that wastewater as an irrigation source was 180 times more harmful to plants than groundwater irrigation, and there were a large number of heavy metals and organic substances in water bodies, which were significantly more carcinogenic to humans than groundwater.

5.2 Atmospheric pollution and human health

VOCs as precursors of ozone $PM_{2.5}$ are not only a serious hazard to the natural ecosystem, but also to the human reproductive, respiratory and blood systems. In addition, atmospheric VOCs are complex and diverse, and in particular, the toxicity of multi-component VOCs coexisting in a system is significantly higher than that of single VOCs [128]. Studies have shown that exposure to VOCs can significantly increase the risk of respiratory disease, asthma and neurological disorders [129]; children living in industrial areas and around cities have a significantly increased risk of leukemia due to exposure to metal industries, hazardous waste and displays treated with organic solvents [130]; and carpeting in cars is a significant source of cancer risk for people who drive for long periods of time [131]. Shuai et al. [132] noted that the concentration of dyeing and finishing industries in the industrial park in Daegu, Korea, led to frequent exposure to volatile organic

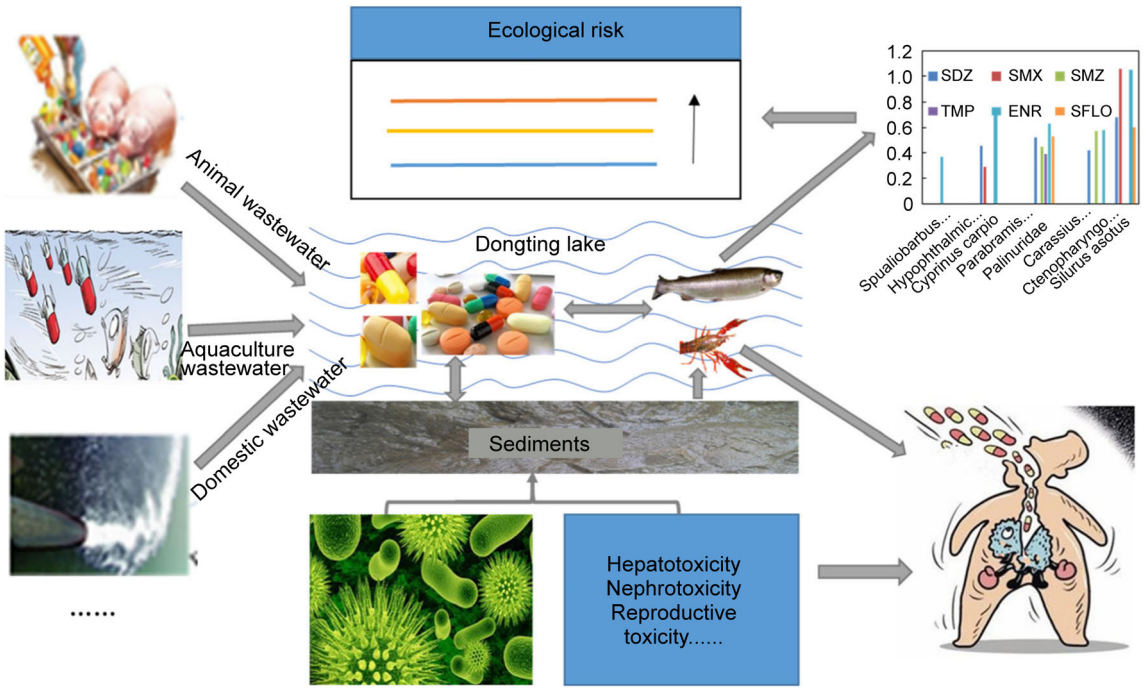

Fig. 21 Pollution and transport of antibiotics in Dongting Lake. Reproduced with permission from Ref. [124]. Copyright 2018, Springer

compounds in the vicinity of the industrial park, which resulted in a significantly higher incidence of respiratory diseases, allergic diseases and cardioembolic diseases in the vicinity of the industrial park than in the control area. Fang et al. [133] pointed out that the levels of formaldehyde, acetaldehyde, and benzene in many households exceed non-cancer risk thresholds, which could harm the respiratory and immune systems, and exacerbate asthma. Hairdressers and beauticians have been reported [134] to have a higher risk of reproductive system disorders, such as infertility, fetal death and preterm birth, than the general population due to their frequent exposure to organic substances such as hair dyes, hairsprays and moisturizers. Researchers have noted that occupational exposure to volatile organic solvents interferes with male reproductive hormones, has toxic effects on male sex steroids, and directly affects testicular function, especially in workers who have been exposed for many years [135]. Zhang et al. [136] explored the effects of kitchen oils (soybean oil, vegetable oil, lard, rapeseed oil, peanut oil and corn oil) on human health (Fig. 22). The study noted that the six oils emitted similar types of VOCs, with vegetable oils emitting more VOCs due to their higher content of unsaturated fatty acids and thus more VOCs. In addition, oil pans would emit higher levels of VOCs as the oil/water ratio increased, and of these VOCs, aldehydes were the most abundant. The risk assessment showed that aldehydes were correlated with the development of lung cancer.

As can be seen from the above, heavy metals and organic pollutants enter the human body through food enrichment, contact or respiratory action, endangering the health of living organisms and even causing carcinogenic, teratogenic and mutagenic effects. Therefore, removing or degrading pollutants through appropriate means not only solves the problem of environmental pollution, but also avoids harm to human health.

6 Conclusion and perspective

The presence of pollutants in water bodies and the atmosphere can lead to environmental problems such as atmospheric photochemical smog, acid rain, haze and eutrophication of water bodies, and can also harm the health of living organisms through respiration or diet, and even produce carcinogenic, teratogenic and mutagenic effects. The UiO-66 series of MOFs are widely used for the adsorption and catalysis of pollutants due to their high specific surface area, rich pore structure, excellent structural stability and semiconductor-like properties. Based on the above properties, the use of UiO-66 and its composites for the adsorption, catalysis or resource recovery of typical pollutants in the environment not only solves the environmental pollution problem, but also enables the resource recovery of pollutants. This review has drawn the following conclusions from the recent research progress of UiO-66 and its composites in environmental purification and resource recovery: the pore structure of the material is adjusted to promote the adsorption and enrichment of pollutants; hydrophobization reduces the competition

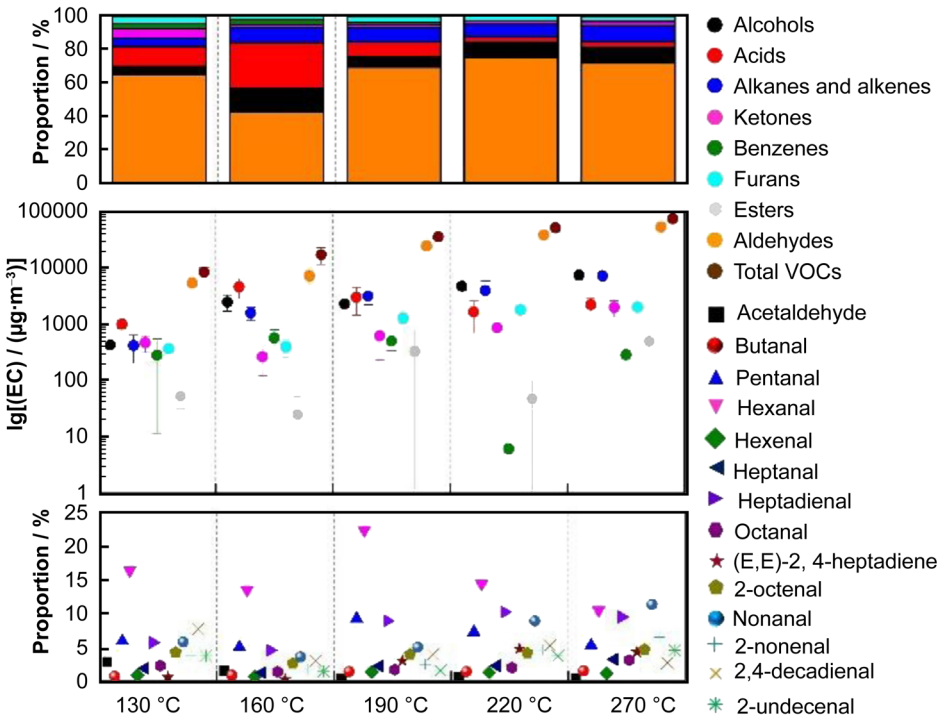

Fig. 22 Relative proportions (upper panel), emission concentrations (middle panel), and speciation and distribution of aldehydes (bottom panel) of soybean oil at different temperatures. Reproduced with permission from Ref. [136]. Copyright 2019, Elsevier

between organic pollutants and water molecules for adsorption; the large specific surface area facilitates not only the dispersion of active sites but also the adsorption of pollutants to achieve effective adsorption of pollutants and complete catalytic oxidation by the active sites. The large specific surface area not only facilitates the dispersion of active sites but also enhances the adsorption of pollutants to achieve effective adsorption and complete catalytic oxidation of pollutants by the active sites.

Although efficient targeted removal or resource utilization of pollutants can be achieved by changing the surface electrical properties, heterojunction composite, or surface modification of materials, there are still some scientific issues that need to be addressed. Firstly, the pH value of actual wastewater varies greatly, and excessively high or low pH values can destroy the structural stability of UiO-66-based materials, which has been rarely studied by researchers. Secondly, the e^{-}-h^{+} recombination of UiO-66-based materials is easy to occur, resulting in poor photocatalytic activity, which is mainly improved through doping, modification, and composite methods. Thirdly, there are many types of pollutants with significant differences in structure and properties, but current research mainly focuses on the removal of single pollutants, and little attention is paid to the simultaneous and efficient removal of multiple components.

Therefore, the future research and development directions of UiO-66-based materials in adsorption, photocatalysis, and resource utilization are as follows: (1) preparing structurally stable MOFs materials to facilitate their long-term application in actual environments; (2) preparing composite materials to break through the selective adsorption of single pollutants by MOFs materials, especially by developing integrated materials that are easy for solid–liquid separation; (3) constructing directional active and adsorption sites to obtain composite materials with integrated adsorption and catalysis, realizing the synergistic mineralization of pollutants; (4) establishing the concept of constructing UiO-66-based materials with single-atom active sites, increasing the catalytic activity of materials while improving their carrier separation.

Acknowledgements This work was financially supported by the National Natural Science Foundation of China (No. 22206080), Zhongyuan Yingcai Jihua (No. ZYYCYU202012183), Henan Key Scientific Research Projects (No. 23B610004), Henan Postdoctoral Foundation (No. 202003027), the Natural Science Youth Fund of Henan Province (Nos. 202300410034 and 232300420336), the Natural Science Foundation of Jiangsu (No. SBK2022041070), the Science and Technology Project of Henan Province (No. 232102321050), the International Science and Technology Cooperation Projects of Henan Province (No. 232102521009), the Young Teacher Foundation of Henan University of Urban Construction (No. YCJQNGGJS202306), China Postdoctoral Science Foundation (No. 2021M701099), the Academic Leader of Henan Institute of Urban Construction (No. YCJXSJSDTR202204), the Science and

Technology Major Special of Pingdingshan (No. 2021ZD03), the Key University Scientific Research Project of Henan Province (No. 22A610007) and the Doctoral Research Start-up Project of Henan University of Urban Construction (No. 990/K-Q2022016).

Declarations

Conflict of interests The authors declare that they have no conflict of interest.

References

[1] Yue K, Zhang XD, Jiang ST, Chen JF, YangY BFK, Wang YX. Recent advances in strategies to modify MIL-125 (Ti) and its environmental applications. J Mol Liq. 2021;335:116108. https://doi.org/10.1016/j.molliq.2021.116108.

[2] Yue XC, Ma NL, Sonne C, Guan RR, Lam SS, Le QV, Chen XM, YangYF GuHP, Rinklebe J, Peng WX. Mitigation of indoor air pollution: a review of recent advances in adsorption materials and catalytic oxidation. J Hazard Mater. 2021;405:124138. https://doi.org/10.1016/j.jhazmat.2020.124138.

[3] Wang JN, Zhao YH, Peng RF, Wang YM, Zhang JH, Zhu XF, Kang HY, Guo CC, Mao YL, Kim JH, Wang CH. When enzyme meet MOFs: emerging opportunities toward water treatment. Chem Eng J. 2023;466:142993. https://doi.org/10.1016/j.cej.2023.142993.

[4] Chen ZS, Li Y, Cai YW, Wang SH, Hu BW, Li BF, Ding XD, Zhuang L, Wang XK. Application of covalent organic frameworks and metal-organic frameworks nanomaterials in organic/inorganic pollutants removal from solutions through sorption-catalysis strategies. Carbon Res. 2023;2(1):8. https://doi.org/10.1007/s44246-023-00041-9.

[5] Zhu B, He SS, Yang Y, Li SW, Lau CH, Liu SM, Shao L. Boosting membrane carbon capture via multifaceted polyphenol-mediated soldering. Nat Commun. 2023;14(1):1697. https://doi.org/10.1038/s41467-023-37479-9.

[6] Usman M, Zeb Z, Ullah H, Suliman MH, Humayun M, Ullah L, Shah SNA, Ahmed U, Saeed M. A review of metal-organic frameworks/graphitic carbon nitride composites for solar--driven green H_2 production, CO_2 reduction, and water purification. J Environ Chem Eng. 2022;10(3):107548. https://doi.org/10.1016/j.jece.2022.107548.

[7] Yang SZ, Li X, Zeng GM, Cheng M, Huang DL, Liu Y, Zhou CY, Xiong WP, Yang Y, Wang WJ, Zhang GX. Materials Institute Lavoisier (MIL) based materials for photocatalytic applications. Coordin Chem Rev. 2021;438:213874. https://doi.org/10.1016/j.ccr.2021.213874.

[8] Bilal M, Rizwan K, Rahdar A, Badran FM, Iqbal MNH. Graphene-based porous nanohybrid architectures for adsorptive and photocatalytic abatement of volatile organic compounds. Environ Pollut. 2022;309:119805. https://doi.org/10.1016/j.envpol.2022.119805.

[9] Maung TZ, Bishop JE, Holt E, Turner MA, Pfrang C. Indoor air pollution and the health of vulnerable groups: a systematic review focused on particulate matter (pm), volatile organic compounds (VOCs) and their effects on children and people with pre-existing lung disease. Int J Environ Res Public Health. 2022;19(14):8752. https://doi.org/10.3390/ijerph19148752.

[10] Liu XL, Li Y, Chen ZS, Yang H, Cai YW, Wang SH, Chen JR, Hu BW, Huang QF, Shen C, Wang XK. Advanced porous nanomaterials as superior adsorbents for environmental pollutants removal from aqueous solutions. Crit Rev Env Sci Tec. 2023;53(13):1289. https://doi.org/10.1080/10643389.2023.2168473.

[11] Liu D, Gu WY, Zhou L, Wang LZ, Zhang JL, Liu YD, Lei JY. Recent advances in MOF-derived carbon-based nanomaterials for environmental applications in adsorption and catalytic degradation. Chem Eng J. 2022;427:131503. https://doi.org/10.1016/j.cej.2021.131503.

[12] Bieniek A, Terzyk AP, Wiśniewski M, Roszek K, Kowalczyk P, Sarkisov L, Keskin S, Kaneko K. MOF materials as therapeutic agents, drug carriers, imaging agents and biosensors in cancer biomedicine: recent advances and perspectives. Prog Mater Sci. 2021;117:100743. https://doi.org/10.1016/j.pmatsci.2020.100743.

[13] Li Y, Huang T, Liu XL, Chen ZS, Yang H, Wang XK. Sorption-catalytic reduction/extraction of hexavalent Cr (VI) and U (VI) by porous frameworks materials. Sep Purif Technol. 2023. https://doi.org/10.1016/j.seppur.2023.123615.

[14] Zhang YQ, Yang F, Sun HG, Bai YP, Li SW, Shao L. Building a highly stable ultrathin nanoporous layer assisted by glucose for desalination. Engineering. 2022;16:247. https://doi.org/10.1016/j.eng.2020.06.033.

[15] He SS, Zhu B, Jiang X, Shao L. Symbiosis-inspired de novo synthesis of ultrahigh MOF growth mixed matrix membranes for sustainable carbon capture. P Nati Acad Sci. 2022;119(1):e2114964119. https://doi.org/10.1073/pnas.2114964119.

[16] Gong YN, Jiao L, Qian YY, Pan CY, Zheng LR, Cai XC, Liu B, Yu SH, Jiang HL. Regulating the coordination environment of MOF-templated single-atom nickel electrocatalysts for boosting CO_2 reduction. Angew Chem. 2020;132(7):2727. https://doi.org/10.1002/ange.201914977.

[17] Guo JL, Liang YH, Liu L, Hu JS, Wang H, An WJ, Cui WQ. Noble-metal-free CdS/Ni-MOF composites with highly efficient charge separation for photocatalytic H_2 evolution. Appl Sur Sci. 2020;522:146356. https://doi.org/10.1016/j.apsusc.2020.146356.

[18] Zhang X, Wang J, Dong XX, Lv YK. Functionalized metal-organic frameworks for photocatalytic degradation of organic pollutants in environment. Chemosphere. 2020;242:125144. https://doi.org/10.1016/j.chemosphere.2019.125144.

[19] Zhang YF, Liu HX, Gao FX, Tan XL, Cai YW, Hu BW, Huang QF, Fang M, Wang XK. Application of MOFs and COFs for photocatalysis in CO_2 reduction, H_2 generation, and environmental treatment. EnergyChem. 2022. https://doi.org/10.1016/j.enchem.2022.100078.

[20] Jansson I, Suárez S, Garcia-Garcia FJ, Sánchez B. Zeolite-TiO_2 hybrid composites for pollutant degradation in gas phase. Appl Catal B Environ. 2015;178:100. https://doi.org/10.1016/j.apcatb.2014.10.022.

[21] Gomes Silva C, Luz I, Llabres i Xamena FX, Corma A. García H (2010) Water stable Zr-benzenedicarboxylate metal-organic frameworks as photocatalysts for hydrogen generation. Chem Eur J. 2010;16(36):11133. https://doi.org/10.1002/chem.200903526.

[22] Katz MJ, Brown ZJ, Colón YJ, Siu PW, Scheidt KA, Snurr RQ, Hupp JT, Farha OK. A facile synthesis of UiO-66, UiO-67 and their derivatives. Chem Commun. 2013;49(82):9449. https://doi.org/10.1039/C3CC46105J.

[23] Vermoortele F, Bueken B, Le BG, Voorde B, Vandichel M, Houthoofd K, Vimont A, Daturi M, Waroquier M, Speybroeck VV, Kirschhock C, De VDE. Synthesis modulation as a tool to increase the catalytic activity of metal-organic frameworks: the unique case of UiO-66 (Zr). J Am Chem Soc. 2013;135(31):11465–8. https://doi.org/10.1021/ja405078u.

[24] Garibay SJ, Cohen SM. Isoreticular synthesis and modification of frameworks with the UiO-66 topology. Chem Commun. 2010;46(41):7700. https://doi.org/10.1039/C0CC02990D.

[25] Cavka JH, Jakobsen S, Olsbye U, Guillou N, Lamberti C, Bordiga S, Lillerud KP. A new zirconium inorganic building

brick forming metal organic frameworks with exceptional stability. J Am Chem Soc. 2008;130(42):13850. https://doi.org/10.1021/ja8057953.
[26] Kandiah M, Nilsen MH, Usseglio S, Jakobsen S, Olsbye U, Tilset M, Larabi C, Quadrelli EA, Bonino F, Lillerud KP. Synthesis and stability of tagged UiO-66 Zr-MOFs. Chem Mater. 2010;22(24):6632. https://doi.org/10.1021/cm102601v.
[27] Li SX, Sun SL, Wu HZ, Wei CH, Hu Y. Effects of electron-donating groups on the photocatalytic reaction of MOFs. Catal Sci Technol. 2018;8(6):1696. https://doi.org/10.1039/C7CY02622F.
[28] Xu JX, Gao JY, Qi YH, Wang C, Wang L. Anchoring Ni_2P on the UiO-66-NH_2/g-C_3N_4-derived C-doped ZrO_2/g-C_3N_4 heterostructure: highly efficient photocatalysts for H_2 production from water splitting. ChemCatChem. 2018;10(15):3327. https://doi.org/10.1002/cctc.201800353.
[29] Wang G, He CT, Huang R, Mao JJ, Wang DS, Li YD. Photoinduction of Cu single atoms decorated on UiO-66-NH_2 for enhanced photocatalytic reduction of CO_2 to liquid fuels. J Am Chem Soc. 2020;142(45):19339. https://doi.org/10.1021/jacs.0c09599.
[30] Wu JF, Fang XX, Zhu YZ, Ma N, Dai W. Well-designed TiO_2@UiO-66-NH_2 nanocomposite with superior photocatalytic activity for tetracycline under restricted space. Energ Fuel. 2020;34(10):12911. https://doi.org/10.1021/acs.energyfuels.0c02485.
[31] Wang SQ, Chen ZS, CaiYW WuXL, Wang SH, Tang ZW, Hu BW, Li Z, Wang XK. Application of COFs in capture/conversion of CO_2 and elimination of organic/inorganic pollutants. Environ Funct Mater. 2023;1:1. https://doi.org/10.1016/j.efmat.2023.03.001.
[32] Ahmadijokani F, Molavi H, Rezakazemi M, Tajahmadi S, Bahi A, Ko F, Aminabhavi TM, Li JR, Arjmand M. UiO-66 metal-organic frameworks in water treatment: a critical review. Prog Mater Sci. 2021. https://doi.org/10.1016/j.pmatsci.2021.100904.
[33] Usman M, Helal A, Abdelnaby MM, Alloush AM, Zeama M, Yamani ZH. Trends and prospects in UiO-66 metal-organic framework for CO_2 capture, separation, and conversion. Chem Rec. 2021;21:1771. https://doi.org/10.1002/tcr.202100030.
[34] Winarta J, Shan B, Mcintyre SM, Ye L, Wang C, Liu JC, Mu B. A decade of UiO-66 research: a historic review of dynamic structure, synthesis mechanisms, and characterization techniques of an archetypal metal-organic framework. Cryst Growth Des. 2019;20(2):1347. https://doi.org/10.1021/acs.cgd.9b00955.
[35] Zou D, Liu D. Understanding the modifications and applications of highly stable porous frameworks via UiO-66. Mater Today Chem. 2019;12:139. https://doi.org/10.1016/j.mtchem.2018.12.004.
[36] Liu QM, Li YY, Chen HF, Lu J, Yu GS, Möslang M, Zhou YB. Superior adsorption capacity of functionalised straw adsorbent for dyes and heavy-metal ions. J Hazard Mater. 2020;382:121040. https://doi.org/10.1016/j.jhazmat.2019.121040.
[37] Vishnu D, Dhandapani B, Kannappan PG, Vo DVN, Ramakrishnan SR. Comparison of surface-engineered superparamagnetic nanosorbents with low-cost adsorbents of cellulose, zeolites and biochar for the removal of organic and inorganic pollutants: a review. Environ Chem Lett. 2021;19(4):3181. https://doi.org/10.1007/s10311-021-01201-2.
[38] Ding ML, Cai XC, Jiang HL. Improving MOF stability: approaches and applications. Chem Sc. 2019;10(44):10209. https://doi.org/10.1039/C9SC03916C.
[39] Ahmadijokani F, Mohammadkhani R, Ahmadipouya S, Shokrgozar A, Rezakazemi M, Molavi H, Aminabhavi TM, Arjmand M. Superior chemical stability of UiO-66 metal-organic frameworks (MOFs) for selective dye adsorption. Chem Eng J. 2020;399:125346. https://doi.org/10.1016/j.cej.2020.125346.
[40] Embaby MS, Elwany SD, Setyaningsih W, Saber RM. The adsorptive properties of UiO-66 towards organic dyes: a record adsorption capacity for the anionic dye Alizarin Red S. Chinese J Chem Eng. 2018;26(4):731. https://doi.org/10.1016/j.cjche.2017.07.014.
[41] Dinh HT, Tran NT, Trinh DX. Investigation into the adsorption of methylene blue and methyl orange by UiO-66-NO_2 nanoparticles. J Anal Methods Chem. 2021. https://doi.org/10.1155/2021/5512174.
[42] Fang X, Wu SB, Wu YH, Yang W, Li YL, He JY, Hong PD, Nie MX, Xie C, Wu ZJ, Zhang KS, Kong LT, Liu JH. High-efficiency adsorption of norfloxacin using octahedral UIO-66-NH_2 nanomaterials: dynamics, thermodynamics, and mechanisms. Appl Sur Sci. 2020;518:146226. https://doi.org/10.1016/j.apsusc.2020.146226.
[43] Zhuang ST, Cheng R, Wang JL. Adsorption of diclofenac from aqueous solution using UiO-66-type metal-organic frameworks. Chem Eng J. 2019;359:354. https://doi.org/10.1016/j.cej.2018.11.150.
[44] Liu L, Cui W, Lu C, Zain A, Zhang W, Shen GX, Hu SQ, Qian XY. Analyzing the adsorptive behavior of Amoxicillin on four Zr-MOFs nanoparticles: Functional groups dependence of adsorption performance and mechanisms. J Environ Manage. 2020;268:110630. https://doi.org/10.1016/j.jenvman.2020.110630.
[45] Wang KN, Wu JJ, Zhu ML, Zheng YZ, Tao X. Highly effective pH-universal removal of tetracycline hydrochloride antibiotics by UiO-66-$(COOH)_2$/GO metal-organic framework composites. J Solid State Chem. 2020;284:121200. https://doi.org/10.1016/j.jssc.2020.121200.
[46] Li SM, Feng F, Chen S, Zhang XL, Liang YX, Shan SS. Preparation of UiO-66-NH_2 and UiO-66-NH_2/sponge for adsorption of 2,4-dichlorophenoxyacetic acid in water. Ecotox Environ Safe. 2020;194:110440. https://doi.org/10.1016/j.ecoenv.2020.110440.
[47] Yang XY, Liu XL, Liu YF, Wang XF, Chen ZS, Wang XK. Optimizing iodine capture performance by metal-organic framework containing with bipyridine units. Front Chem Sci Eng. 2023;17(4):395. https://doi.org/10.1007/s11705-022-2218-3.
[48] Yang WX, Cheng MJ, Han Y, Luo XL, Li CH, Tang WZ, Yue TL, Li ZH. Heavy metal ions' poisoning behavior-inspired etched UiO-66/CTS aerogel for Pb (II) and Cd (II) removal from aqueous and apple juice. J Hazard Mater. 2021;401:123318. https://doi.org/10.1016/j.jhazmat.2020.123318.
[49] Peng D, Liu ZY, Su XY, Xiao YQ, Wang YC, Middletond BA, Lei T. Spatial distribution of heavy metals in the West Dongting Lake floodplain. China Environ Sci-Proc Imp. 2020;22(5):1256. https://doi.org/10.1039/C9EM00536F.
[50] Wang H, Wang S, Wang SX, Zhang LB, Zhou Y, Yang F. Efficient and selective removal of Cr(VI) by the modified UiO-66-NH_2 with phenothiazine-N-rhodanine from aqueous solution: performance and mechanisms. Micropor Mesopor Mat. 2022;336:111834. https://doi.org/10.1016/j.micromeso.2022.111834.
[51] Tang JL, Chen YB, Zhao MH, Wang SX, Zhang LB. Phenylthiosemicarbazide-functionalized UiO-66-NH_2 as highly efficient adsorbent for the selective removal of lead from aqueous solutions. J Hazard Mater. 2021;413:125278. https://doi.org/10.1016/j.jhazmat.2021.125278.
[52] Liu JM, Cui HH, Li JH, Chen MC. A research on the cadmium ions adsorption of Sulfhydryl-and sulfo-functionalized UIO-66

with silica layer from water. J Environ Chem Eng. 2021;9(1):104621. https://doi.org/10.1016/j.jece.2020.104621.
[53] Huang LTY, Cao H, Ma JZ, Wang XX. Efficient removal of Pb (II) by UiO-66-NH_2: a combined experimental and spectroscopic studies. Environ Nanotechnol Monit Manage. 2022;18:100741. https://doi.org/10.1016/j.enmm.2022.100741.
[54] Wu Y, Xie YH, Liu XL, Li Y, Wang JY, Chen ZS, Yang H, Hu BW, Shen C, Tang ZW, Huang QF, Wang XK. Functional nanomaterials for selective uranium recovery from seawater: material design, extraction properties and mechanisms. Coordin Chem Rev. 2023;483:215097. https://doi.org/10.1016/j.ccr.2023.215097.
[55] Zhong J, Liu XY, Zhang MJ, Yan X, Hu XW. Research progress of bioremediation technology for uranium contamination. Chin J Rare Met. 2021;45(1):93. https://doi.org/10.13373/j.cnki.cjrm.xy19040039.
[56] Peng RF, Zhang S, Yao YY, Wang JN, Zhu XF, Jiang R, Zhang JH, Zhang W, Wang CH. MOFs meet electrospinning: new opportunities for water treatment. Chem Eng J. 2023;453:139669. https://doi.org/10.1016/j.cej.2022.139669.
[57] Zhao B, Yuan LY, Wang Y, Duan T, Shi WQ. Carboxylated UiO-66 tailored for U (VI) and Eu (III) trapping: from batch adsorption to dynamic column separation. ACS Appl Mater Inter. 2021;13(14):16300. https://doi.org/10.1021/acsami.1c00364.
[58] Li SY, Jin YY, Hu ZQ, Liu Y, Wu SY, Wang Y, Wang GH. Performance and mechanism for U (VI) adsorption in aqueous solutions with amino-modified UiO-66. J Radioanal Nucl Ch. 2021;330:857. https://doi.org/10.1007/s10967-021-07968-6.
[59] Gumber N, Pai RV, Sanyal K, Dutta B, Hassan PA. Synthesis and uranium adsorption studies of UiO-66 (Ce) based metal organic frameworks from aqueous solutions. Micropor Mesopor Mat. 2022;341:112108. https://doi.org/10.1016/j.micromeso.2022.112108.
[60] Wen MC, Li GY, Liu HL, Chen JY, An TC, Yamashita H. Metal-organic framework-based nanomaterials for adsorption and photocatalytic degradation of gaseous pollutants: recent progress and challenges. Environ Sci-Nano. 2019;6(4):1006. https://doi.org/10.1039/C8EN01167B.
[61] Li XQ, Zhang L, Yang ZQ, Wang P, Yan YF, Ran JY. Adsorption materials for volatile organic compounds (VOCs) and the key factors for VOCs adsorption process: a review. Sep Purif Technol. 2020;235:116213. https://doi.org/10.1016/j.seppur.2019.116213.
[62] Vo TK, Le VN, Yoo KS, Song M, Kim D, Kim J. Facile synthesis of UiO-66 (Zr) using a microwave-assisted continuous tubular reactor and its application for toluene adsorption. Cryst Growth Des. 2019;19(9):4949. https://doi.org/10.1021/acs.cgd.9b00170.
[63] Vo TK, Nguyen VC, Song M, Kim D, Yoo KS, Park BJ, Kim J. Microwave-assisted continuous-flow synthesis of mixed-ligand UiO-66 (Zr) frameworks and their application to toluene adsorption. J Ind Eng Chem. 2020;86:178. https://doi.org/10.1016/j.jiec.2020.03.001.
[64] Vellingiri K, Kumar P, Deep A, Kim KH. Metal-organic frameworks for the adsorption of gaseous toluene under ambient temperature and pressure. Chem Eng J. 2017;307:1116. https://doi.org/10.1016/j.cej.2016.09.012.
[65] Hasan Z, Tong M, Jung BK, Ahmed I, Zhong C, Jhung SH. Adsorption of pyridine over amino-functionalized metal-organic frameworks: attraction via hydrogen bonding versus base-base repulsion. J Phys Chem C. 2014;118(36):21049. https://doi.org/10.1021/jp507074x.
[66] Zhou L, Zhang XH, Chen YL. Modulated synthesis of zirconium metal-organic framework UiO-66 with enhanced dichloromethane adsorption capacity. Mater Lett. 2017;197:167. https://doi.org/10.1016/j.matlet.2017.03.162.
[67] Ou R, Zhu WJ, Li LL, Wang XY, Wang Q, Gao Q, Yuan AH, Pan JM, Yang F. Boosted capture of volatile organic compounds in adsorption capacity and selectivity by rationally exploiting defect-engineering of UiO-66(Zr). Sep Purif Technol. 2021;266:118087. https://doi.org/10.1016/j.seppur.2020.118087.
[68] Zhang XD, Yang Y, Song L, Chen JF, Yang YQ, Wang YX. Enhanced adsorption performance of gaseous toluene on defective UiO-66 metal organic framework: equilibrium and kinetic studies. J hazard Mater. 2019;365:597. https://doi.org/10.1016/j.jhazmat.2018.11.049.
[69] Zhang XD, Lv XT, Shi XY, Yang Y, Yang YQ. Enhanced hydrophobic UiO-66 (University of Oslo 66) metal-organic framework with high capacity and selectivity for toluene capture from high humid air. J colloid interf Sci. 2019;539:152. https://doi.org/10.1016/j.jcis.2018.12.056.
[70] Shi XY, Zhang XD, Bi FK, Zheng ZH, Sheng LJ, Xu JC, Wang Z, Yang YQ. Effective toluene adsorption over defective UiO-66-NH_2: an experimental and computational exploration. J Mol Liq. 2020;316:113812. https://doi.org/10.1016/j.molliq.2020.113812.
[71] Zhang XD, Shi XY, Chen JF, Yang Y, Lu G. The preparation of defective UiO-66 metal organic framework using MOF-5 as structural modifier with high sorption capacity for gaseous toluene. J Environ Chem Eng. 2019;7(5):103405. https://doi.org/10.1016/j.jece.2019.103405.
[72] Hu P, Liang XP, Yaseen M, Sun XD, Tong ZF, Zhao ZX, Zhao ZX. Preparation of highly-hydrophobic novel N-coordinated UiO-66(Zr) with dopamine via fast mechano-chemical method for (CHO-/Cl-)-VOCs competitive adsorption in humid environment. Chem Eng J. 2018;332:608. https://doi.org/10.1016/j.cej.2017.09.115.
[73] Sun DR, Adiyala PR, Yim SJ, Kim DP. Pore-surface engineering by decorating metal-oxo nodes with phenylsilane to give versatile super-hydrophobic metal-organic frameworks (MOFs). Angew Chem. 2019;131(22):7483. https://doi.org/10.1002/ange.201902961.
[74] Zhang DC, Liu JJ, Wang C, Liu Y, Wang JH, Han X. Application of metal-organic frameworks in the purification of indoor hexanal: experiments and DFT calculations. Build Environ. 2020;182:107095. https://doi.org/10.1016/j.buildenv.2020.107095.
[75] You SZ, Hu Y, Liu XC, Wei CH. Synergetic removal of Pb (II) and dibutyl phthalate mixed pollutants on Bi_2O_3-TiO_2 composite photocatalyst under visible light. Appl Catal B-Environ. 2018;232:288. https://doi.org/10.1016/j.apcatb.2018.03.025.
[76] Huang QQ, Hu Y, Pei Y, Zhang JH, Fu ML. In situ synthesis of TiO_2@NH_2-MIL-125 composites for use in combined adsorption and photocatalytic degradation of formaldehyde. Appl Catal B-Environ. 2019;259:118106. https://doi.org/10.1016/j.apcatb.2019.118106.
[77] Jin JC, Yang M, Zhang YL, Dutta A, Xie CG, Kumar A. Integration of mixed ligand into a multivariate metal-organic framework for enhanced UV-light photocatalytic degradation of Rhodamine B. J Taiwan Inst Chem E. 2021;129:410. https://doi.org/10.1016/j.jtice.2021.08.041.
[78] Mu XX, Jiang JF, Chao FF, Lou YB, Chen JX. Ligand modification of UiO-66 with an unusual visible light photocatalytic behavior for RhB degradation. Dalton T. 2018;47(6):1895. https://doi.org/10.1039/C7DT04477A.
[79] Bibi R, Shen QH, Wei LF, Hao DD, Li NX, Zhou JC. Hybrid BiOBr/UiO-66-NH_2 composite with enhanced visible-light driven photocatalytic activity toward RhB dye degradation. RSC adv. 2018;8(4):2048. https://doi.org/10.1039/c7ra11500h.

[80] Liang Q, Cui SN, Liu CH, Xu S, Yao C, Li ZY. Construction of CdS@UIO-66-NH_2 core-shell nanorods for enhanced photocatalytic activity with excellent photostability. J colloid interf Sci. 2018;524:379. https://doi.org/10.1016/j.jcis.2018.03.114.
[81] Abdi J, Yahyanezhad M, Sakhaie S, Vossoughi M, Alemzadeh I. Synthesis of porous TiO_2/ZrO_2 photocatalyst derived from zirconium metal organic framework for degradation of organic pollutants under visible light irradiation. J Environ Chem Eng. 2019;7(3):103096. https://doi.org/10.1016/j.jece.2019.103096.
[82] Yang ZQ, Tong XW, Feng JN, He S, Fu ML, Niu XJ, Zhang TP, Liang H, Ding A, Feng XC. Flower-like BiOBr/UiO-66-NH_2 nanosphere with improved photocatalytic property for norfloxacin removal. Chemosphere. 2019;220:98. https://doi.org/10.1016/j.chemosphere.2018.12.086.
[83] Cao J, Yang ZH, Xiong WP, Zhou YY, Peng YR, Li X, Zhou CY, Xu R, Zhang YR. One-step synthesis of Co-doped UiO-66 nanoparticle with enhanced removal efficiency of tetracycline: simultaneous adsorption and photocatalysis. Chem Eng J. 2018;353:126. https://doi.org/10.1016/j.cej.2018.07.060.
[84] Zhao C, Li Y, Chu HY, Pan X, Ling L, Wang P, Fu HF, Wang CC, Wang ZH. Construction of direct Z-scheme Bi_5O_7I/UiO-66-NH_2 heterojunction photocatalysts for enhanced degradation of ciprofloxacin: mechanism insight, pathway analysis and toxicity evaluation. J Hazard Mater. 2021;419:126466. https://doi.org/10.1016/j.jhazmat.2021.126466.
[85] Testa JJ, Grela MA, Litter MI. Heterogeneous photocatalytic reduction of chromium (VI) over TiO_2 particles in the presence of oxalate: involvement of Cr(V) species. Environ Sci Technol. 2004;38(5):1589. https://doi.org/10.1021/es0346532.
[86] Upadhyay U, Sreedhar I, Singh SA, Patel CM, Anitha KL. Recent advances in heavy metal removal by chitosan based adsorbents. Carbohyd Polym. 2021;251:117000. https://doi.org/10.1016/j.carbpol.2020.117000.
[87] Li ZW, Wang L, Qin L, Lai C, Wang ZH, Zhou M, Xiao LH, Liu SY, Zhang MM. Recent advances in the application of water-stable metal-organic frameworks: adsorption and photocatalytic reduction of heavy metal in water. Chemosphere. 2021;285:131432. https://doi.org/10.1016/j.chemosphere.2021.131432.
[88] He J, Zhou HL, Peng QM, Wang YT, Chen YJ, Yan ZY, Wang JQ. UiO-66 with confined dyes for adsorption and visible-light photocatalytic reduction of aqueous Cr (VI). Inorg Chem Commun. 2022;140:109441. https://doi.org/10.1016/j.inoche.2022.109441.
[89] Wei X, Wang CC, Li Y, Wang P, Wei Q. The Z-scheme NH_2-UiO-66/PTCDA composite for enhanced photocatalytic Cr (VI) reduction under low-power LED visible light. Chemosphere. 2021;280:130734. https://doi.org/10.1016/j.chemosphere.2021.130734.
[90] Du XD, Yi XH, Wang P, Zheng WW, Deng JG, Wang CC. Robust photocatalytic reduction of Cr (VI) on UiO-66-NH_2 (Zr/Hf) metal-organic framework membrane under sunlight irradiation. Chem Eng J. 2019;356:393. https://doi.org/10.1016/j.cej.2018.09.084.
[91] Li ZF, Zhang ZB, Dong ZM, Yu FT, Ma MY, Wang YC, Wang YQ, Liu YH, Liu J, Cao XH, Liu YH. Solar light-responsive CdS/UiO-66-NH_2 for ultrafast uranium reduction from uranium-containing mine wastewater without external sacrificial agents. Sep Purif Technol. 2022;283:120195. https://doi.org/10.1016/j.seppur.2021.120195.
[92] Dong DP, Yan CX, Huang JD, Lu N, Wu PY, Wang J, Zhang ZY. An electron-donating strategy to guide the construction of MOF photocatalysts toward co-catalyst-free highly efficient photocatalytic H_2 evolution. J Mater Chem A. 2019;7(42):24180. https://doi.org/10.1039/C9TA06141J.
[93] Yao PZ, Liu HL, Wang DT, Chen JY, Li GY, An TC. Enhanced visible-light photocatalytic activity to volatile organic compounds degradation and deactivation resistance mechanism of titania confined inside a metal-organic framework. J Colloid Interf Sci. 2018;522:174. https://doi.org/10.1016/j.jcis.2018.03.075.
[94] Zhang JH, Hu Y, Qin JX, Yang ZX, Fu ML. TiO_2-UiO-66-NH_2 nanocomposites as efficient photocatalysts for the oxidation of VOCs. Chem Eng J. 2020;385:123814. https://doi.org/10.1016/j.cej.2019.123814.
[95] Zhang JH, Guo ZY, Yang ZX, Wang J, Xie J, Fu ML, Hu Y. TiO_2@UiO-66 composites with efficient adsorption and photocatalytic oxidation of VOCs: investigation of synergistic effects and reaction mechanism. ChemCatChem. 2021;13(2):581. https://doi.org/10.1002/cctc.202001466.
[96] Yan X, Liu XY, Zhang MJ, Cui XL, Zhong J, Hu XW. Research progress of biosorption technology for chromium contamination. Chin J Rare Met. 2021;45(2):240. https://doi.org/10.13373/j.cnki.cjrm.xy19060028.
[97] Sin SN, Chua H, Lo W, Ng LM. Assessment of heavy metal cations in sediments of Shing Mun River. Hong Kong Environ Int. 2001;26(5–6):297. https://doi.org/10.1016/S0160-4120(01)00003-4.
[98] Shim J, Lim JM, Shea PJ, Oh BT. Simultaneous removal of phenol, Cu and Cd from water with corn cob silica-alginate beads. J hazard Mater. 2014;272:129. https://doi.org/10.1016/j.jhazmat.2014.03.010.
[99] Xu JJ, Gu HY, Chen MD, Li XP, Zhao HW, Yang HB. Dual Z-scheme Bi_3TaO_7/Bi_2S_3/SnS_2 photocatalyst with high performance for Cr (VI) reduction and TC degradation under visible light irradiation. Rare Met. 2022;41(7):2417. https://doi.org/10.1007/s12598-022-01988-1.
[100] Zeng HJ, Yu ZX, Shao LY, Li XH, Zhu M, Liu YC, Feng XF, Zhu XM. Ag_2CO_3@UiO-66-NH_2 embedding graphene oxide sheets photocatalytic membrane for enhancing the removal performance of Cr (VI) and dyes based on filtration. Desalination. 2020;491:114558. https://doi.org/10.1016/j.desal.2020.114558.
[101] Zhou YC, Xu XY, Wang P, Fu HF, Zhao C, Wang CC. Facile fabrication and enhanced photocatalytic performance of visible light responsive UiO-66-NH_2/Ag_2CO_3 composite. Chinese J Catal. 2019;40(12):1912. https://doi.org/10.1016/S1872-2067(19)63433-9.
[102] Zhao C, Zhang Y, Jiang H, Chen J, Liu Y, Liang Q, Zhou M, Li Z, Zhou Y. Combined effects of octahedron NH_2-UiO-66 and flowerlike $ZnIn_2S_4$ microspheres for photocatalytic dye degradation and hydrogen evolution under visible light. J Phys Chem C. 2019;123(29):18037.
[103] Cao MT, Yang FL, Zhang Q, Zhang JH, Zhang L, Li LF, Wang XH, Dai WL. Facile construction of highly efficient MOF-based Pd@UiO-66-NH_2@$ZnIn_2S_4$ flower-like nanocomposites for visible-light-driven photocatalytic hydrogen production. J Mater Sci Technol. 2021;76:189. https://doi.org/10.1016/j.jmst.2020.11.028.
[104] Wei QM, Xiong SX, Li W, Jin C, Chen YS, Hou LL, Wu ZL, Pan ZL, He QY, Wang YZ, Tang DY. Double Z-scheme system of α-$SnWO_4$/UiO-66(NH_2)/g-C_3N_4 ternary heterojunction with enhanced photocatalytic performance for ibuprofen degradation and H_2 evolution. J Alloy Comp. 2021;885:160984. https://doi.org/10.1016/j.jallcom.2021.160984.
[105] Shi JW, Chen F, Hou LL, Li GS, Li YQ, Guan XJ, Liu HP, Guo LJ. Eosin Y bidentately bridged on UiO-66-NH_2 by solvothermal treatment towards enhanced visible-light-driven photocatalytic H_2 production. Appl Catal B-Environ. 2021;280:119385. https://doi.org/10.1016/j.apcatb.2020.119385.

[106] Tian P, He X, Zhao L, Li WX, Fang W, Chen H, Zhang FQ, Huang ZH, Wang HL. Enhanced charge transfer for efficient photocatalytic H_2 evolution over UiO-66-NH_2 with annealed $Ti_3C_2T_x$ MXenes. Int J Hydrogen Energy. 2019;44(2):788. https://doi.org/10.1016/j.ijhydene.2018.11.016.
[107] Sun K, Liu M, Pei JZ, Li DD, Ding CM, Wu KF, Jiang HL. Incorporating transition-metal phosphides into metal-organic frameworks for enhanced photocatalysis. Angew Chem. 2020; 132(50):22937. https://doi.org/10.1002/ange.202011614.
[108] Wang XJ, Yang GR, Chai GD, Nasir MS, Wang SL, Zheng X, Wang CY, Yan W. Fabrication of heterostructured UIO-66-NH_2/CNTs with enhanced activity and selectivity over photocatalytic CO_2 reduction. Int J Hydrogen Energy. 2020; 45(55):30634. https://doi.org/10.1016/j.ijhydene.2020.08.273.
[109] Zhou AQ, Yang JM, Zhu XW, Zhu XL, Liu JY, Liu JY, Zhong K, Chen HX, Chu JY, Du YS, Song YH, Qiao JC, Li HM, Xu H. Self-assembly construction of NiCo LDH/ultrathin g-C_3N_4 nanosheets photocatalyst for enhanced CO_2 reduction and charge separation mechanism study. Rare Met. 2022;41(6): 2118. https://doi.org/10.1007/s12598-022-01960-z.
[110] Aresta M, Dibenedetto A, Angelini A. Catalysis for the valorization of exhaust carbon: from CO_2 to chemicals, materials, and fuels technological use of CO_2. Chem Rev. 2014;114(3): 1709.
[111] Wan SP, Ou M, Zhong Q, Wang XM. Perovskite-type CsPbBr3 quantum dots/UiO-66(NH_2) nanojunction as efficient visible-light-driven photocatalyst for Co_2 reduction. Chem Eng J. 2019;358:1287. https://doi.org/10.1016/j.cej.2018.10.120.
[112] Wang XJ, Yang GR, Chai GD, Nasir MS, Wang SL, Zheng X, Wang CY, Yan W. Fabrication of heterostructured UIO-66-NH2/CNTs with enhanced activity and selectivity over photocatalytic CO2 reduction. Int J Hydrog Energy 2020; 45(55):30634–46. https://doi.org/10.1016/j.ijhydene.2020.08.273.
[113] Zhao XX, Xu MY, Song XH, Zhou WQ, Liu X, Yan Y, Huo PW. Charge separation and transfer activated by covalent bond in UiO-66-NH_2/RGO heterostructure for CO_2 photoreduction. Chem Eng J. 2022;437:135210. https://doi.org/10.1016/j.cej.2022.135210.
[114] Hu SC, Deng ZS, Xing MY, Wu SQ, Zhang JL. Highly dispersed cobalt centers on UiO-66-NH_2 for photocatalytic CO_2 reduction. Catal Lett. 2022. https://doi.org/10.1007/s10562-022-04081-5.
[115] Khoshnava SM, Rostami R, Mohamad ZR, Štreimikienė D, Mardani A, Ismail M. The role of green building materials in reducing environmental and human health impacts. Int J environ Res public health. 2020;17(7):2589. https://doi.org/10.3390/ijerph17072589.
[116] Adamová T, Hradecký J, Pánek M. Volatile organic compounds (VOCs) from wood and wood-based panels: methods for evaluation, potential health risks, and mitigation. Polymers. 2020;12(10):2289. https://doi.org/10.3390/polym12102289.
[117] Liang ZS, Wang JJ, Zhang YN, Han C, Ma ST, Chen JY, Li GY, An TC. Removal of volatile organic compounds (VOCs) emitted from a textile dyeing wastewater treatment plant and the attenuation of respiratory health risks using a pilot-scale biofilter. J Clean Prod. 2020;253:120019. https://doi.org/10.1016/j.jclepro.2020.120019.
[118] Li S, Shi WZ, Liu W, Li HM, Zhang W, Hu JR, Ke YC, Sun WL, Ni JR. A duodecennial national synthesis of antibiotics in China's major rivers and seas (2005–2016). Sci Total Environ. 2018;615:906. https://doi.org/10.1016/j.scitotenv.2017.09.328.
[119] Liang XM, Chen BW, Nie XP, Shi Z, Huang XP, Li XD. The distribution and partitioning of common antibiotics in water and sediment of the Pearl River Estuary. South China Chemosphere. 2013;92(11):1410. https://doi.org/10.1016/j.chemosphere.2013.03.044.
[120] Sun Q, Lv M, Hu AY, Yang XY, Yu CP. Seasonal variation in the occurrence and removal of pharmaceuticals and personal care products in a wastewater treatment plant in Xiamen. China J hazard Mater. 2014;277:69. https://doi.org/10.1016/j.jhazmat.2013.11.056.
[121] Verheij C, Rood PPM, Deelstra CK, Levendag MLL, Koch BCP, Polinder S, Schuit SCE, Haagsma JA. Emergency department visits due to intoxications in a Dutch university hospital: occurrence, characteristics and health care costs. PLoS ONE. 2019;14(12):e0226029. https://doi.org/10.1371/journal.pone.0226029.
[122] Tang JF, Sun J, Wang WD, Yang L, Xu YY. Pharmaceuticals in two watersheds in Eastern China and their ecological risks. Environ Pollut. 2021;277:116773. https://doi.org/10.1016/j.envpol.2021.116773.
[123] Duan L, Zhang YZ, Wang B, Zhou YT, Wang F, Sui Q, Xu DJ, Yu G. Seasonal occurrence and source analysis of pharmaceutically active compounds (PhACs) in aquatic environment in a small and medium-sized city. China Sci Total Environ. 2021;769:144272. https://doi.org/10.1016/j.scitotenv.2020.144272.
[124] Liu XH, Lu SY, Meng W, Zheng BH. Residues and health risk assessment of typical antibiotics in aquatic products from the Dongting Lake, China-"Did you eat 'Antibiotics' today?" Environ Sci Pollut Res. 2018;25(4):3913. https://doi.org/10.1007/s11356-017-0745-0.
[125] Ayadi I, Souissi Y, Jlassi I, Peixoto F. Chemical synonyms, molecular structure and toxicological risk assessment of synthetic textile dyes: a critical review. J Dev Drugs. 2016;5(151): 2. https://doi.org/10.4172/2329-6631.1000151.
[126] Winpenny J, Heinz I, Koo-Oshima S, Salgot M, Collado J, Hernández F, Torricelli R. The wealth of waste: the economics of wastewater use in agriculture. Water Rep. 2010;35:129.
[127] Muhammad N, Nafees M, Ge L, Haya KM, Bilal M, Chan WP, Lisak G. Assessment of industrial wastewater for potentially toxic elements, human health (dermal) risks, and pollution sources: a case study of Gadoon Amazai industrial estate, Swabi. Pakistan J Hazard Mater. 2021;419:126450. https://doi.org/10.1016/j.jhazmat.2021.126450.
[128] Fiedler N, Laumbach R, Kelly-McNeil K, Lioy P, Fan ZH, Jf Z, Ottenweller J, Ohman-Strickland P, Kipen H. Health effects of a mixture of indoor air volatile organics, their ozone oxidation products, and stress. Environ Health Persp. 2005; 113(11):1542. https://doi.org/10.1289/ehp.8132.
[129] Herbarth O, Matysik S. Decreasing concentrations of volatile organic compounds (VOC) emitted following home renovations. Indoor Air. 2010;20(2):141. https://doi.org/10.1111/j.1600-0668.2009.00631.x.
[130] García-Pérez J, López-Abente G, Gómez-Barroso D, Morales-Piga A, Romaguera EP, Tamayo I, Fernández-Navarro P, Ramis R. Childhood leukemia and residential proximity to industrial and urban sites. Environ Res. 2015;140:542. https://doi.org/10.1016/j.envres.2015.05.014.
[131] Liang B, Yu X, Mi HP, Liu D, Huang QQ, Tian M. Health risk assessment and source apportionment of VOCs inside new vehicle cabins: a case study from Chongqing. China Atmos Pollut Res. 2019;10(5):1677. https://doi.org/10.1016/j.apr.2019.06.008.
[132] Shuai JF, Kim SS, Ryu H, Park J, Lee CK, Kim GB, Ultra JVU, Yang W. Health risk assessment of volatile organic compounds exposure near Daegu dyeing industrial complex in South Korea. BMC Public Health. 2018;18(1):1. https://doi.org/10.1186/s12889-018-5454-1.

[133] Fang L, Norris C, Johnson K, Cui XX, Sun JQ, Teng YB, Tian E, Xu W, Li Z, Mo JH, Schauer JJ, Black M, Bergin M, Zhang J, Zhang YP. Toxic volatile organic compounds in 20 homes in Shanghai: concentrations, inhalation health risks, and the impacts of household air cleaning. Build Environ. 2019;157:309. https://doi.org/10.1016/j.buildenv.2019.04.047.

[134] Kim D, Kang MY, Choi S, Park J, Lee HJ, Kim EA. Reproductive disorders among cosmetologists and hairdressers: a meta-analysis. Int Arch Occ Env Hea. 2016;89(5):739. https://doi.org/10.1007/s00420-016-1112-z.

[135] Eldesouki MA, Sharaf NE, Shakour AAA, Mohamed MS, Hussein AS, Hasani IW. Study of the effect of occupational exposure to volatile organic compounds (VOC's) on male reproductive hormones. World J Med Sci. 2013;8(1):6. https://doi.org/10.5829/idosi.wjms.2013.8.1.1112.

[136] Zhang DC, Liu JJ, Jia LZ, Wang P, Han X. Speciation of VOCs in the cooking fumes from five edible oils and their corresponding health risk assessments. Atmos Environ. 2019;211:6. https://doi.org/10.1016/j.atmosenv.2019.04.043.